LIFE AFTER CHOPS: THE ALASKAN HEAVY OIL RESERVOIR PERSPECTIVE

By

Bakul Mathur

A Thesis Submitted in Partial Fulfillment of the Requirements

for the Degree of

Master of Science

in

Petroleum Engineering

University of Alaska Fairbanks

May 2017

APPROVED:

Dr. Abhijit Dandekar, Committee Chair

Dr. Santanu Khataniar, Committee Co-chair

Dr. Shirish Patil, Committee Member

Dr. Abhijit Dandekar, Chair

Department of Petroleum Engineering

Dr. Douglas Goering, Dean

College of Engineering and Mines

Dr. Michael Castellini, *Dean of the Graduate School*

Abstract

The heavy oil reservoirs in Alaska offer major production challenges, including proximity to the permafrost layer, very high viscosity oil and low mechanical strength pay zones. The Ugnu deposits of the Alaska North Slope (ANS) hold more than 6 billion barrels of oil. The dead oil viscosity at reservoir temperature ranges from 1,000 to 1,000,000 cp[1]. In an effort to sustain well life, this research focuses on the unique set of challenges occurring in the Ugnu reservoir and presents the best possible way to maximize production.

The present research accentuates observations derived from the field data, which shows that deliberate sand production with the hydrocarbon stream while employing a Progressive Cavity Pump (PCP) as an artificial lift method has a favorable effect on primary oil recovery. The developments have led to the advent of a technique called Cold Heavy Oil Production with Sand (CHOPS) as an initial production method for shallow heavy oil reservoirs. Sand production leads to the formation of high porosity channels or wormholes that can range up to hundreds of meters. The co-mingling of heavy oil and sand develops foamy oil by creating a bubbly flow inside the reservoir. The combination of these wormholes with the foamy oil behavior are the primary factors that result in enhanced production during CHOPS. One of the major hindrances to its successful application is the selection of the post-CHOPS production method, which is addressed in this study with the help of modeling and simulation.

Alternative recovery techniques following the primary cold production include water flooding, polymer injection, miscible gas injection and thermal recovery methods. Water flooding is unviable because of the mobility contrast between the highly viscous oil and water. The high permeability zones provide a bypass for water, consequently producing elevated water cuts.

Another aspect unique to Alaskan heavy oil reservoirs is the proximity to the permafrost layer, with the hydrocarbon bearing zone making thermal recovery methods unappealing. Polymer injection and miscible gas injection become the favorable non-thermal secondary and tertiary recovery methods in this case.

This study is based on modeling one of the wells drilled into the M80 sands of the Ugnu formation followed by the analysis of post-CHOPS recovery for the well. The CHOPS well modeling is done with the help of a wormhole fractal pattern and a foamy oil model. Simulation of the polymer injection is then employed from a nearby well. The results indicate almost 12% increment in recovery with polymer flooding as compared to the natural depletion. The recovery obtained from the simulations have been analyzed to provide a basis for designing the polymer injection job as an Enhanced Oil Recovery (EOR) method after CHOPS. With the promising results of this study, it can be determined that the Ugnu reservoir sands can be exploited for heavy oil with the help of polymer flooding. It can also be combined with miscible gas flooding or alkali-surfactant flooding to obtain even higher hydrocarbon recoveries.

Dedication

To my beloved parents, loving sister and affectionate family.

Table of Contents

List of Figures

Page

List of Tables

Page

Acknowledgements

I would like to thank the University of Alaska Fairbanks (UAF) and the Department of Petroleum Engineering for giving me an opportunity to conduct my research and providing financial support for my graduate studies.

I am highly indebted to my committee chair, Dr. Abhijit Dandekar and committee co-chair Dr. Santanu Khataniar, for steering me in the right direction whenever they thought I needed it. The door to Dr. Dandekar's office was always open whenever I ran into a trouble spot or had a question about my research or writing. I am grateful to Dr. Khataniar for his patience and support in overcoming numerous obstacles I have been facing through my research.

I wish to thank Dr. Shirish Patil for the time he spent with me as a member for this thesis. Dr. Patil provided valuable assistance when needed from King Fahd University of Petroleum and Minerals (KFUPM) in Saudi Arabia, where he is now Saudi Aramco Chair Professor of Petroleum Engineering. His assistance and contributions, even though there was a 12 hour difference in time zones, are highly appreciated. Also, I would like to thank KFUPM for allowing Dr. Patil to dedicate his time towards this effort.

I am grateful to Dr. Debasmita Misra, Department of Residence Life, Department of Mathematics and Statistics for always being supportive in helping me fund myself through on-campus student jobs for an appreciable amount of my student tenure.

I would like to acknowledge Dr. Catherine Hanks, Mr. Kushagra Saxena, Mr. Kiran Venepalli, Mr. Benjamin Siks, and Mr. Anthony McConkey for helping me with my research either by providing software support or generously giving the field data essential for my research. I am thankful to all my friends at UAF for keeping my energy up during my stay in Fairbanks.

Finally, I must express my very profound gratitude to my parents, Mr. Govind Mathur and Mrs. Abha Mathur, my sister Anindya, Abhay Jiju and to my dearest friends Vivek Bhardwaj and Arya Narayan for providing me with unfailing support and continuous encouragement throughout my years of study and through the process of researching and writing this thesis. This accomplishment would not have been possible without them. Thank you.

CHAPTER 1 INTRODUCTION

Heavy oil is an abundant source of energy. However, its production is more challenging and expensive compared to light or conventional oil thanks to its very high viscosity. The post-production processing of heavy oil further adds to the cost. However, in recent years, increasing demand for oil and technological developments have made heavy oil a viable resource.

Heavy oil is defined as a liquid petroleum that has less than 20° API gravity[1] or more than 200 cp viscosity at reservoir conditions. Heavy oil reservoirs are typically comprised of weak and unconsolidated sandstone and exist at shallow depths. These reservoirs have high porosity (28-36%), and viscosity of the heavy oil ranges from 500 to 15,000 cp[1]. Heavy oils originate as light oil and after migration to shallower traps, they undergo biodegradation and turn into heavy oil. Heavy oil reservoirs differ from one another depending upon the fluid quality and rock properties; therefore, the methods of heavy oil recovery vary considerably from one reservoir to another. Heavy oil in Venezuela and Canada constitutes around 35% of the total world heavy oil reserves followed by the Middle East, US and Russia, as shown in Figure 1:

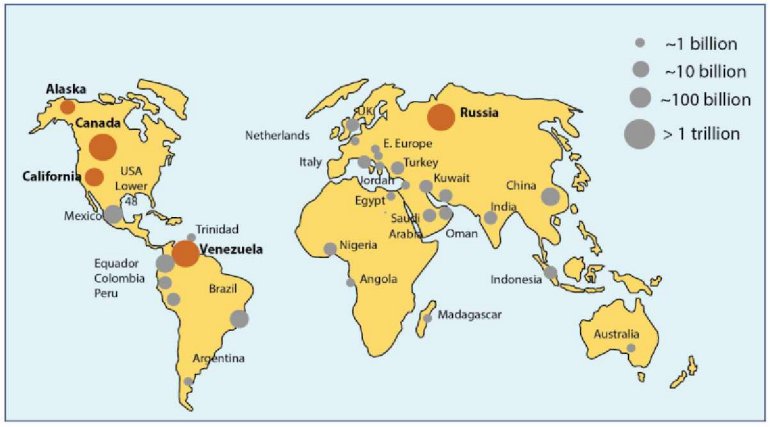

Figure 1: World oil reserves[2]

The abundance of heavy oil in the Arctic region has led to the development of numerous tertiary recovery processes, but the presence of permafrost in these cold areas poses a unique challenge for producing such viscous oil, making thermal recovery processes unviable.

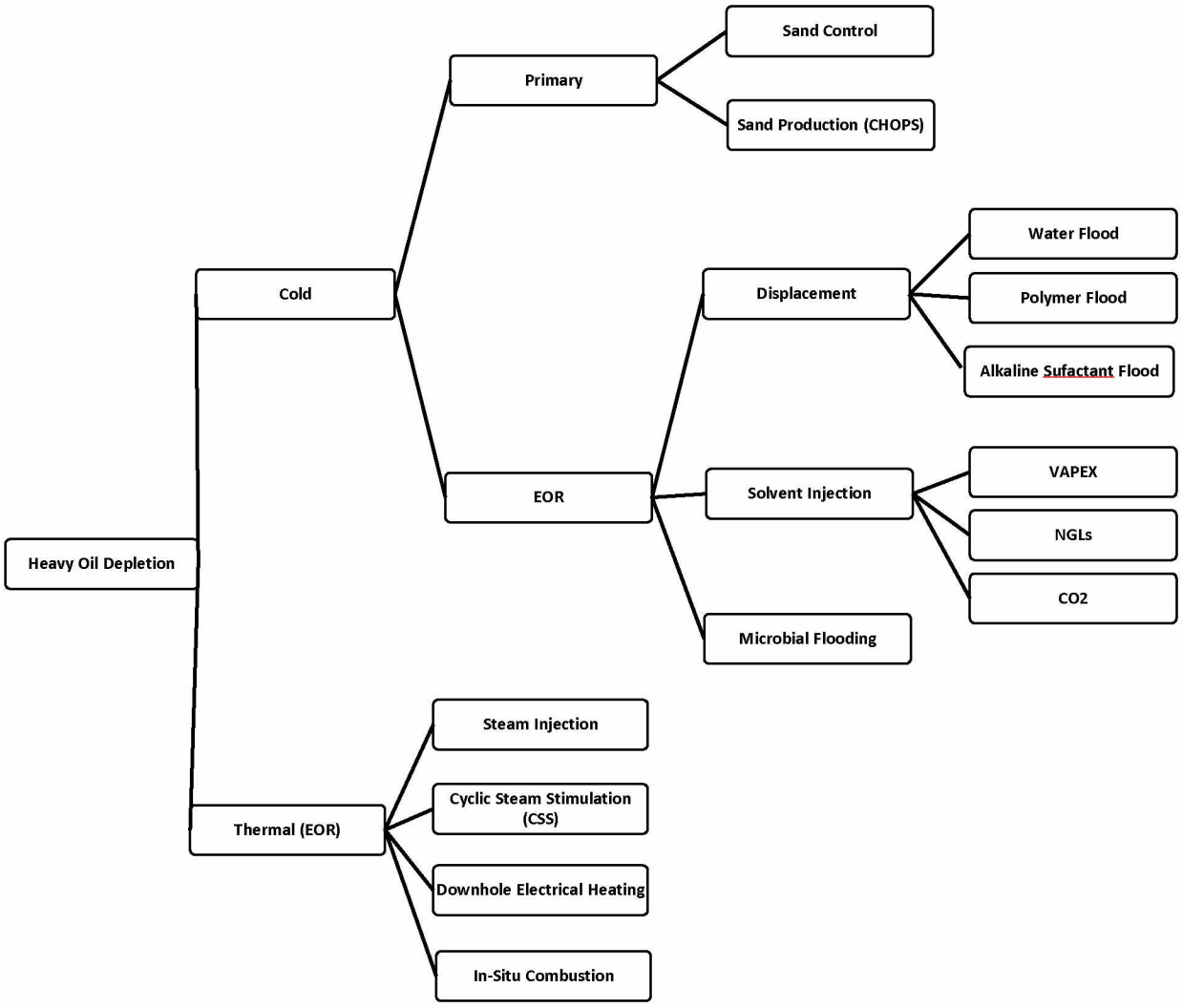

Figure 2: Heavy oil depletion techniques[3]

Figure 2 shows the depletion techniques developed to date for heavy oil reservoirs. Water flooding has been applied conventionally in most of the heavy oil reservoirs having dead oil viscosities up to 2000 cp[4].

1.1 Alaska's Heavy Oil Potential

The Prudhoe Bay, Kuparuk River and Milne Point fields in Alaska's North Slope basin hold some of the largest oil reserves in North America. The Ivishak reservoir in the Prudhoe Bay field and the Kuparuk reservoirs in the Kuparuk River and Milne Point Units have historically produced conventional light oil. Apart from the well-known conventional oil reserves, the North Slope of Alaska holds a vast resource of heavy oil in shallow sands overlying these conventional reservoirs (see Figure 3). The cold shallow sands in the Milne Point, Kuparuk River and Prudhoe Bay fields have between 24 and 33 billion bbl of heavy oil[5].

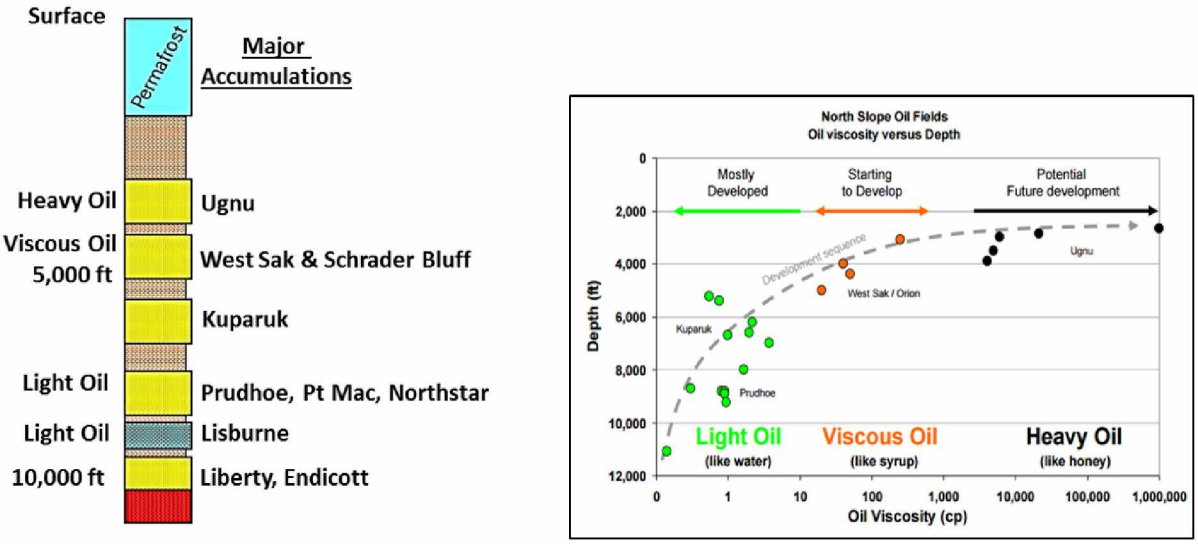

Figure 3: Generalized stratigraphic column for Alaska North Slope; Oil viscosity range for major reservoirs[6]

The Ugnu sands account for 12 to 18 billion bbl of this heavy oil resource. Ugnu heavy oil accumulation was discovered in 1969 while targeting a deeper conventional oil formation in the present day Milne Point field[7]. This accumulation of heavy to extra heavy oil occurs at depths from 610 m to 1524 m (2,000 ft to 5,000 ft) true vertical depth. The API gravity range of Ugnu oil is between 14 and 8 API, with corresponding live oil viscosities ranging from 300 to 50,000 cp. The initial gas/oil ratios range from 200 scf/stb to less than 50 scf/stb. The gas is 95% methane[5]. The oil becomes progressively heavier towards the west because of higher biodegradation.

In Alaska, the oil industry's focus has conventionally been on the light oil from deeper reservoirs. For example, production techniques for the viscous oil accumulations of West Sak and Schrader Bluff are under development, while the shallow depth, heavy oil sands of Ugnu remain underdeveloped, owing to the extremely high in-situ viscosities ranging from 1,000 to 1,000,000 cp[2]. The oil-in-place estimate of the Ugnu deposit approximates to 21 billion barrels, of which 5 to 10 percent is considered technically (but not yet economically) recoverable[8]. To demonstrate the technical viability of heavy oil production from Ugnu, a pilot project was initiated in 2011. In this project, two horizontal wells in the Milne point field targeting the Ugnu M sands were drilled to appraise the Ugnu formation and were installed with surface-driven progressive cavity pumps (PCP) to initiate sand influx. Figure 4 shows the relative location of the Milne Point unit and the extent of the Ugnu reservoir. In the limited period of production, both the wells produced around 20% of sand cut with oil rates higher than theoretically calculated from the given horizontal sections. Further production was, however, hindered since significant technological and investment challenges did not allow the operators to maintain economical flow rates. Thus, this pilot project facility is under a shutdown awaiting further development. Cold heavy oil production

and the subsequent enhanced recovery techniques demand extensive research before the production activities can be resumed in the project area.

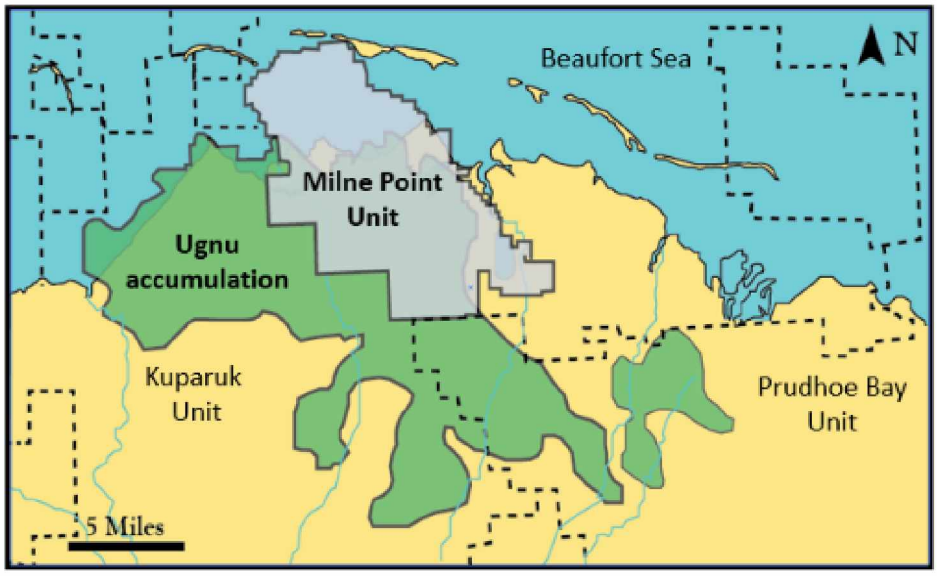

Figure 4: Location map of Milne Point Unit and extent of Ugnu accumulation[5]

Post-CHOPS recovery methods are of the utmost importance to enhancing oil production. Thermal EOR methods, though being the most efficient heavy oil recovery techniques, are not advisable for the arctic environment, especially in the Ugnu reservoir, because of its proximity to the permafrost layer. Besides the environmental concerns, a laboratory study by Hallam et al.[9] showed that at high temperatures, the Ugnu sands undergo a drastic reduction in permeability due to pore throat plugging with an oil-wet material. Also, the high mobility of the water phase may adversely affect the production performance because of cyclic steam stimulation[9]. Considering the limitations of thermal recovery processes and the higher mobility of low viscosity injection fluids like water or gas, polymer injection seems to be the most viable option to improve oil recovery from the Ugnu sands.

1.2 Cold Heavy Oil Production with Sand (CHOPS)

CHOPS is one of the primary and field-driven production methods and has proven its potential for improving the overall recovery of the heavy oil present in the cold, shallow, unconsolidated reservoirs. CHOPS has been applied with very good success to enhance heavy oil production in Canada, China, Venezuela and Kazakhstan[10].

In this method, a deliberate initiation and maintenance of sand production is carried out, generally with the help of a progressive cavity pump. A typical CHOPS production cycle is 6 to 30 months, which is comprised of high initial flow rates followed by slow decay and reduction in reservoir energy. This cycle is often followed by a work-over to reestablish oil and sand production.

CHOPS can increase oil production by 5 to 20 times and oil recovery by 12 to 20% original oil in place (OOIP). This drastic enhancement in production and recovery is mainly associated with increased conductivity in the reservoir. Large drawdown pressures created with the help of progressive cavity pumps help in releasing high amounts of gas bubbles from the heavy oil. These gas bubbles are stabilized with an asphaltene covering and do not form a continuous gas phase, giving rise to a "foamy oil flow"[11]. This foamy behavior increases the oil's mobility. Being at shallower depths, the heavy oil reservoirs are generally unconsolidated, and, therefore, the mobility of the oil causes a failure of the friable reservoir rock. The fine rock grains flow with the foamy oil, creating irregularly shaped high permeability channels inside the reservoir. These channels are called "wormholes." Various experiments have been performed to analyze the wormholes' properties. These wormholes act as a negative skin and have porosities as high as 65% that help prevent the near wellbore area from being blocked with precipitated asphaltene, mineral deposits or fine-grained particles[11]. Wormholes are generated at the wellbore and can extend even

up to hundreds of meters depending upon the mechanical strength of the reservoir rock (see Figure 5).

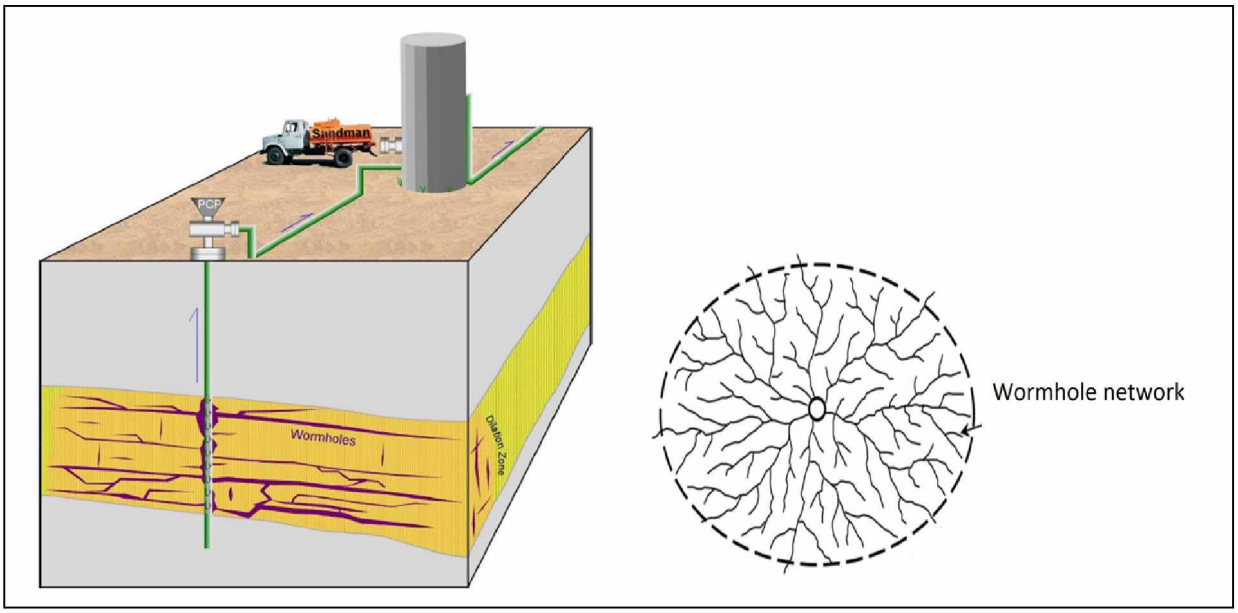

Figure 5: Wormhole propagation in reservoir[3]

The complex multiphase mixture (oil, gas, water and sand) flows through these wormholes into the wellbore. During the flow, some of the sand gets settled down inside these high porosity channels and creates two distinct regions of porous media – a lower region with settled sand that has higher porosity than the original reservoir matrix and the upper region of almost 100% porosity, in which the fluid flow takes place.

After a certain period, the wormhole halts expansion, marking the beginning of the second phase of the CHOPS process. In this phase, the main source of the produced sand is the settled sand that is scoured out of the high porosity, high permeability channels.

The presence of wormhole channels is confirmed by tracer tests, rapid interval communications, linear-flow well signatures, seismic surveys and laboratory observations[12-22]. These channels are

very helpful in providing a conductive path for heavy oil during primary production; however, for subsequent waterflooding, these channels act as bypass routes for the injected water, leading to poor oil recoveries. Being a recently developed technique, understanding of the pore scale phenomenon involved in the CHOPS process is still in its nascent stage, and thus various techniques for modeling and simulation of CHOPS are still being developed and verified. Reasonably accurate modeling of CHOPS enables the user to simulate, plan and carry out the secondary and tertiary heavy oil recovery operations.

1.3 Research Structure

This research consists of three distinct modeling and simulation stages (see Figure 6). In the first stage, a base model was constructed and simulated for CHOPS production. Specifically, the Milne Point horizontal wells MPS-41A and MPS-39 were modeled in the M80T reservoir layer using the contour map. The reservoir fluid was modeled in CMG-Winprop using the PVT lab report. A wormhole network was then developed for production well MPS-41A, and the well was simulated for production. A satisfactory match between the actual well and simulated well oil, gas and water productions was achieved by varying the simulation parameters. The history match validated the base model.

In the second stage, the base model was used for simulations of post-CHOPS recovery techniques. For reference, the model well (MPS-41A) was first produced without applying any EOR techniques, i.e., depleted. Next, the reservoir was flooded with water. Horizontal well MPS-39 was used as the injection well.

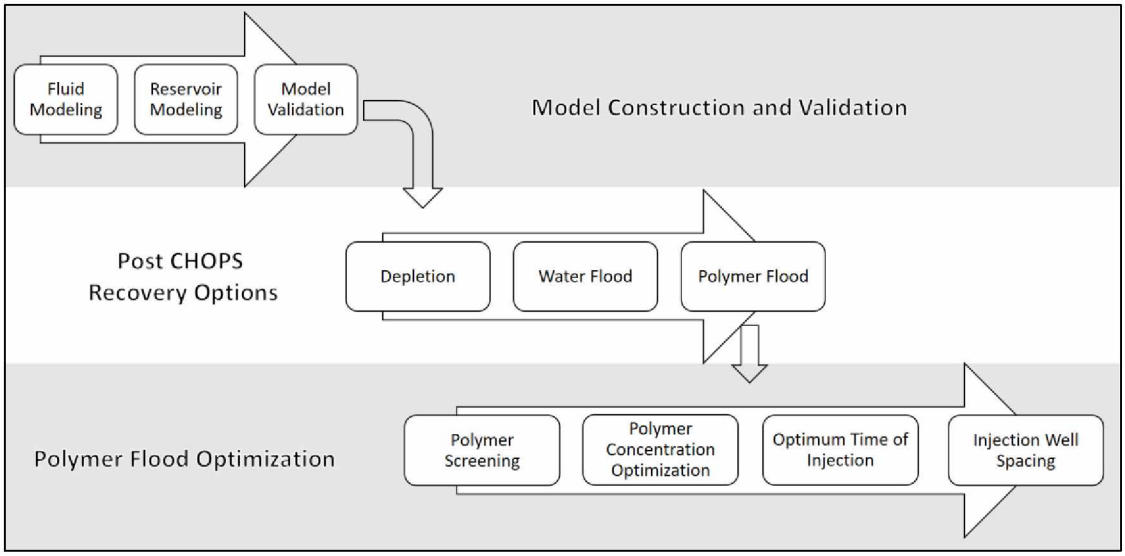

Figure 6: Research structure

The third stage of the research consisted of optimizing the polymer flooding scheme. The polymer flood was optimized for the type of polymer, polymer concentration, optimum time of injection and injection well spacing. The size of the polymer slug was not determined in this research. Conclusions are based on the optimized polymer injection program for the reservoir modeled in this study.

CHAPTER 2 LITERATURE REVIEW

2.1 Ugnu Geology

The shallow sands of ANS comprise the Ugnu and West Sak formations (see Figure 7). Ugnu sands are mainly a stacked fluvial sequence deposited in the Late Cretaceous and Early Tertiary marine and deltaic environment. The Ugnu sands are oriented in east-west direction and show vertical and areal heterogeneity. The strata dips at about 2 degree from southwest to northeast with thick pay zones occurring from 2,200 to 3,200 ft[9].

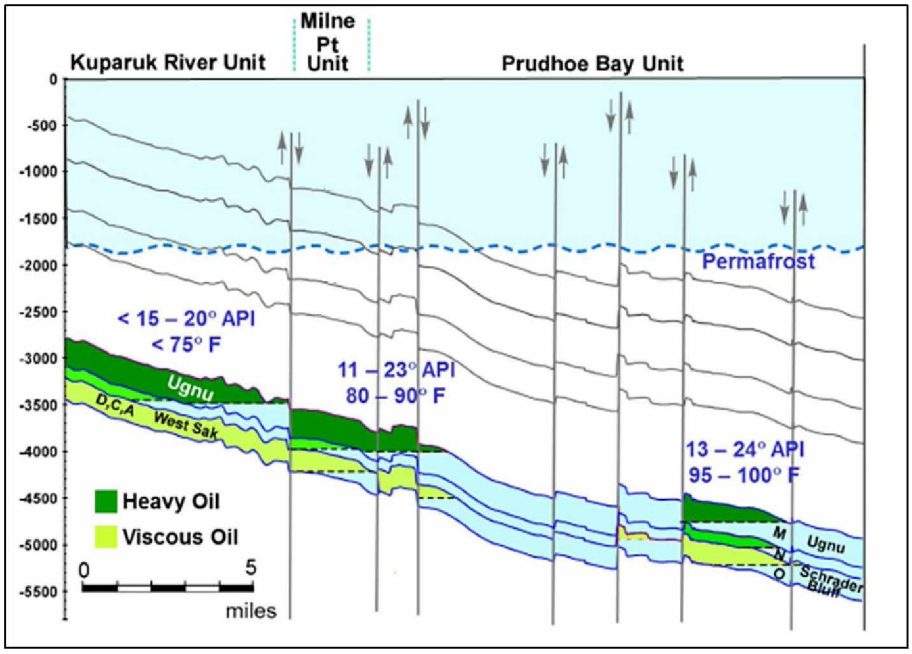

Figure 7: Ugnu, Schrader Bluff and West Sak with multiple thin horizons, local oil-water contacts, varied depth and oil quality[6]

The Ugnu formation is cut by normal faults. The oil viscosity in the Ugnu reservoir is primarily affected by the proximity of the permafrost layer. Permafrost is a thick layer of soil typically found in Polar Regions that stays frozen year-round. Melting of the permafrost layer puts strain on the well casing structure. Therefore, it plays a key role in developing the Ugnu reservoir. Within the

area that contains thick Ugnu accumulations, the permafrost thickness averages to about 1,650 ft. The temperature of the base of the permafrost is about 31 degrees F[9]. Potential hydrate zones exist within and near the base of permafrost.

2.2 Significant Recovery Mechanisms of CHOPS

More factors contribute to the higher flow rate in the CHOPS process than are predicted by conventional Darcy's law. The main mechanisms that lead to higher oil recoveries in CHOPS are as follows:

- Enhancement of porosity and permeability due to sand removal from the formation as well as any mechanical skin that may have developed. The concept of the wormhole was formulated from field experiences of communication channels between distant wellbores after sand production[22,23,24]. These channels are developed due to sand liquefaction caused by high pressure gradients. The liquefied region propagates into the reservoir to create increased porosity and permeability zones named wormholes. Wormholes tend to grow within preferred layers of low mechanical strength. Sand production remains continuous and substantial in the wormhole channels.
- Increase in oil flow velocity relative to fixed coordinates owing to the mobilization of rock matrix. Experimental results indicate that the heavy oil is fluxed into the tip of wormhole and the sand is liquefied[1]. The high sand content slurry flows toward the wellbore through wormholes, and the sand transport directly enhances the fluid flow rate. The slurry flow inside the wormhole channel can also be considered a multiphase pipe flow. The high viscosity and aggressive pressure gradient keeps the sand liquefaction continuous with high concentrations of sand toward the tip of the permeable channel. The sand transport acts as

a blockage clean up mechanism by removing the pore throat blockages. Flow enhancement is observed due to the apparent negative skin development[1].

- Flow enhancement due to expansion of entrapped gas bubbles in the foamy oil where gas does not form a continuous phase. Large drawdown induced during CHOPS leads to gas ex-solution in the form of bubbles. These bubbles take a longer time to coalesce than predicted by conventional solution gas flow formulations because of the oil's high viscosity. Therefore, less gas is evolved out of the heavy oil. Most of the gas bubbles remain entrained inside the asphaltene covering. This entrained gas provides internal drive resulting in a higher liquid velocity. The heavy oil with entrapped gas bubbles is called foamy or bubbly oil. A sample of what foamy oil looks like is shown in Figure 8.

Figure 8: Foamy oil sample[25]

- Easier formation compression because of higher porosity leading to a compaction drive. Before the generation of high porosity channels, the strata successfully carry the overburden. During aggressive sand production, the unconsolidated reservoir undergoes shear and dilation, inducing compaction of the overlaying rocks. At this stage, the overburden is supported by inter-well "pillars"[26]. The overall rock compressibility is

significantly increased after the wormhole channels are fully developed, which acts as a compaction drive.

2.3 Modeling the CHOPS Process

CHOPS is relatively unexplored primary production technique. Since it is driven by field experiences, the simulation front is still in its nascent stage in terms of both the geo-mechanical and fluid flow aspects. Owing to the multiple mechanisms involved in the CHOPS process, it is generally difficult to encompass them all in a single simulation study. The compaction drive mechanism is omitted in most of the CHOPS models due to relatively lower impact on the overall enhancement in oil production. Similarly, the multiphase flow of the oil, water, gas and sand slurry mixture is an extremely complicated modeling challenge. This section discusses the various modeling and simulation methods for CHOPS used by different researchers.

2.3.1 Modeling Wormhole Propagation

Continuous sand production in CHOPS results in dynamic alterations in reservoir properties, making dynamic geological modeling necessary. The drastic porosity and permeability enhancement is the biggest focus when modeling CHOPS. Different perspectives have been proposed to explain the voids created due to the sand production. As per the widely accepted wormhole theory, the growth of the wormhole network progresses with the production of sand. These high permeability channels can even connect different wells that are tens of miles away[22]. Per one theory, a dilated zone of altered porosity is created around the wellbore, which extends with continuous sand production[27]. However, field experience has shown that wells drilled farther away have experienced mud loss because they hit a wormhole channel, thereby confirming the wormhole network theory[27]. Figure 9 explains why the wormhole theory is accepted over the dilated zone theory.

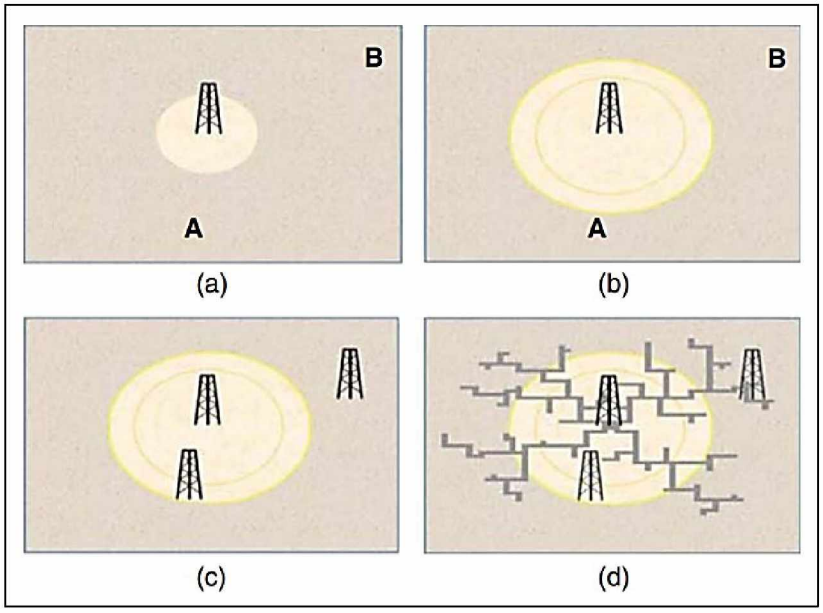

Figure 9: Representation of possible wormhole networks: (a) CHOPS well on production; (b) Developed dilated region; (c) Based on dilated region theory, well A should see an altered zone but not well B; (d) Field experience shows well A does not see the altered zone, but well B does, supporting the existence of wormholes.[27]

Modeling wormhole propagation is rather challenging due to its dependency on the mechanical strength of the rock matrix. A precise wormhole propagation is very difficult to model without knowledge of the areal heterogeneity of the sand body. Different approaches have been used by different authors to simulate this process. One approach for modeling translates the sand production into an enhanced permeability zone around the wellbore. Another approach by Denbina et al.[28] used a transmissibility multiplier to dynamically increase the permeability with an increase in pressure depletion. While this approach is easier to model, it does not take the wormhole fractal pattern in consideration, especially when a homogeneous reservoir is modeled. The modeling processes can be majorly divided into two types: geo-mechanical models and probabilistic models.

While geo-mechanical models tackle the physics of wormhole propagation, the probabilistic models take the random nature of the wormholes in account.

2.3.1.1 Geo-mechanical Models

The physics of wormhole generation and propagation involves various geo-mechanical factors, like mechanical strength of the rock matrix, reservoir fluid velocity and pressure gradient at the tip of an individual wormhole. The sanding propagation model developed by Han et al.[10] assumed a difference in rock mechanical behavior between an elastic region and a region where elastoplastic behavior, including dilation, is taking place. This model depicts the extent of the wormhole propagation using Mohr-Coulomb yield criterion based on the effective radial and tangential stresses on the rock sample. The wormhole grows if the pressure gradient at the tip of the wormhole is greater than that determined by the rock properties. Although, more accurately, these models are difficult to use in practice because they require a huge amount of reservoir rock data and enormous computational time.

2.3.1.2 Probabilistic Models

Based on the fundamental assumption that wormhole networks can represent random behavior, the CHOPS reservoir model can be generated using a probabilistic approach. If the reservoir rock mechanical data is unavailable, this assumption is quite satisfactory. A certain degree of randomness exists in the direction followed by a wormhole because of variations in the cohesive strength within a formation, but wormhole patterns can still be generated using the probabilistic approach with statistical tools. One of the examples of probabilistic modeling is the Probabilistic Active Walker (PAW) model. In this model, the walker modifies the landscape surrounding it while walking, in turn influencing the walker's decision for the next step[29]. The wormhole growth

generated by the probabilistic method can be periodically updated and adjusted based on seismic data or other information if available[27].

2.3.2 Fluid Modeling

Equations of state (EOS) are used in commercial simulators to model the pressure, volume and temperature (PVT) laboratory experimental data for hydrocarbon fluids. Peng-Robinson[30] (PR) is one of the most common EOSs used in the oil industry. The explicit form of the PR EOS in terms of pressure is given by:

$$P = \frac{RT}{\tilde{v} - b} - \frac{\alpha a}{\tilde{v} + 2b\tilde{v} - b^2} \tag{1}$$

Where

$$\alpha = [1 + (0.37464 + 1.54226\omega - 0.2699\omega^2)(1 - \sqrt{T_r})]^2 \tag{2}$$

$$a = 0.45724\frac{R^2T_c^2}{P_c} \tag{3}$$

$$b = 0.07780\frac{RT_c}{P_c} \tag{4}$$

Coefficients "a" and "b" are functions of the critical properties T_c (critical temperature) and P_c (critical pressure), T_r is reduced temperature and ω is called the acentric factor. The equation was developed for pure components, but with the help of the mixing rules, lumped components can also be simulated using the PR EOS. The mixing rules are given by Equations (5) and (6).

$$(\alpha a)_m = \sum\sum y_i y_j \alpha_{ij} = \sqrt{(\alpha a)_i (\alpha a)_j}(1 - k_{ij}) \tag{5}$$

$$b_m = \sum_i y_i b_i \tag{6}$$

The subscript "m" defines the mixture properties. The binary interaction coefficient k_{ij} is tuned to better fit the experimental data.

Foamy oil behavior is the second recovery contributor in heavy oil reservoirs. As mentioned earlier, foamy oil is generated due to entrapment of gas bubbles in the oil phase constrained in the asphaltene layer. These gas bubbles expand and move with the oil velocity, causing the oil to swell. A significant number of the gas bubbles do not fuse into the continuous gas phase and remain isolated. High oil recovery, low producing GOR and natural pressure maintenance are the distinguishing features of foamy oil.

Simulating foamy oil can be done with four different modeling techniques. Various parameters can be adjusted in these models to match the production history. The key parameters are critical gas saturation, oil/gas relative permeability, fluid and/or rock compressibility, pressure depletion oil viscosity and absolute permeability.

2.3.2.1 Pseudo Bubble Point Model

Kraus et al.[31] developed the pseudo bubble point method to simulate the foamy oil primary production. This method uses modified fluid properties to imitate the delayed coalescence of gas bubbles. The solution gas remains entrapped in the reservoir fluid until the pressure reaches the pseudo or modified bubble point pressure. This approach enables the solution drive to act for much longer than in the fluid with the actual bubble point pressure by enhancing the apparent fluid compressibility.

2.3.2.2 Modified Fractional Flow Model

In this model, described by Lebel[32], the fractional flow curve is modified to obtain the desired gas flow. The fractional flow of gas increases as gas saturation increases, until a limiting gas saturation is reached. The model suggests altering the relative permeability of a portion of the gas phase.

2.3.2.3 Reduced Viscosity Model

This model lowers the fluid viscosity for simulation purposes. Claridge and Prats[33] postulated the reduced viscosity theory, which suggests that the heavy oil loses its viscosity when asphaltene is adhered to the gas bubbles leaving the oil phase. This phenomenon has not been verified experimentally.

2.3.2.4 Non-equilibrium Reaction Model

The non-equilibrium reaction model developed by Geilikman et al.[34] team assumes a pseudo component in the fluid model representing the gas bubbles. These gas bubbles are generated from the lower hydrocarbons present in the oil. The bubble generation process is irreversible, denoting entrapment. The physical properties of the "bubble" component are set to be the same as the hydrocarbon component from which it was generated.

2.4 Enhanced Oil Recovery (EOR) After CHOPS

After the primary and secondary recovery mechanisms, further production enhancement techniques are required to maintain sustainable production. This can be done through several EOR techniques like water flooding, gas injection, chemical injection, polymer flooding, etc.

2.4.1 Water Flooding

Water flooding is the conventional EOR method employed in the North Slope and is further aided by availability of low salinity water from the Prince Creek aquifer, making water flooding an inexpensive and convenient option.

While water flooding is a standard EOR method for light oil, it is not recommended for heavy and extra heavy oil reservoirs because of the unfavorable mobility ratio between the injected water and reservoir fluid. As an outcome of this adverse mobility ratio, the injected water bypasses the native reservoir fluid, creating a finger-like flow pattern, as shown in Figure 10, and leaving a large amount of oil unswept. This phenomenon is called viscous fingering. Viscous fingering hinders the complete displacement of oil with water in reservoirs, thereby rendering water flooding ineffective.

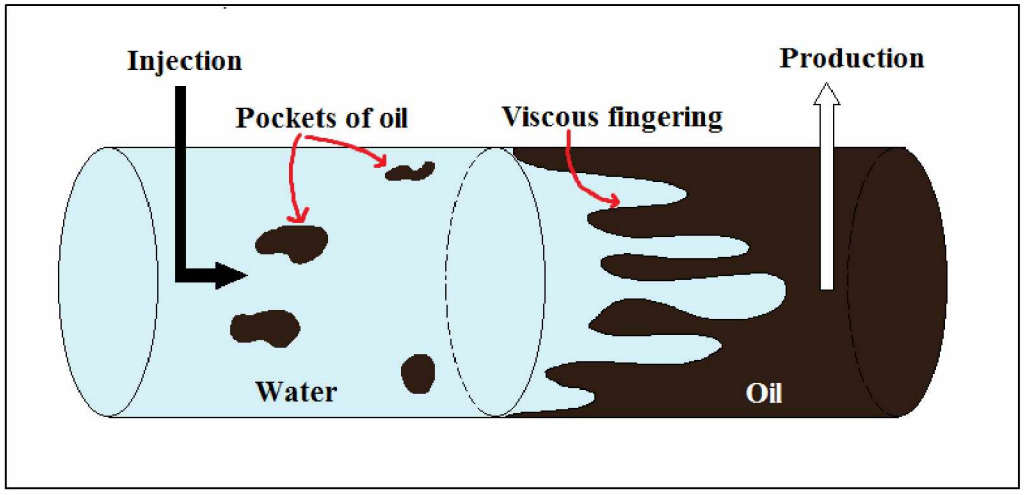

Figure 10: Water flooding in heavy oil reservoir

Mobility ratio (M) is defined as the ratio of mobility of the displacing fluid to the mobility of the displaced fluid, where mobility is the ratio of the effective permeability (κ) with the viscosity (μ)

of the same phase. When water is the displacing fluid, the mobility ratio can be described as in Equation (7).

$$M = \frac{(k_{rw})\mu_o}{(k_{ro})\mu_w} \quad (7),$$

where k_{rw} and k_{ro} are water relative permeability and oil relative permeability, μ_w and μ_o are water and oil viscosities, respectively.

The ratio is an indication of the stability of a displacement process. Values less than or equal to 1 are the desired values for mobility ratio for an effective sweep (M<=1). A value of M over 1 indicates unstable displacement. The mobility ratio and the volumetric sweep efficiency are inversely proportional to each other. A higher value of mobility ratio represents a higher difference in viscosity of the fluids involved. One way of overcoming this is to use polymers, which increases the viscosity of the displacing fluid.

2.4.2 Polymer Flooding

The EOR method of polymer flooding is carried out to enhance the production by lowering the mobility ratio within the reservoir. Polymer flooding is the prime candidate when dealing with highly heterogeneous reservoirs, e.g., unconsolidated sandstone and high water flood mobility ratios, which includes heavy oil reservoirs. The standard polymer flooding procedure, shown in Figure 11, includes pumping water into the reservoir as a preflush. The preflush water also conditions the reservoir by balancing the reservoir's salinity. Since polymer solutions are sensitive to salinity, a low salinity preflush water is recommended, followed by pumping the polymer with water until the optimum slug size is achieved, then further followed by water injection as a drive to produce the displaced oil.

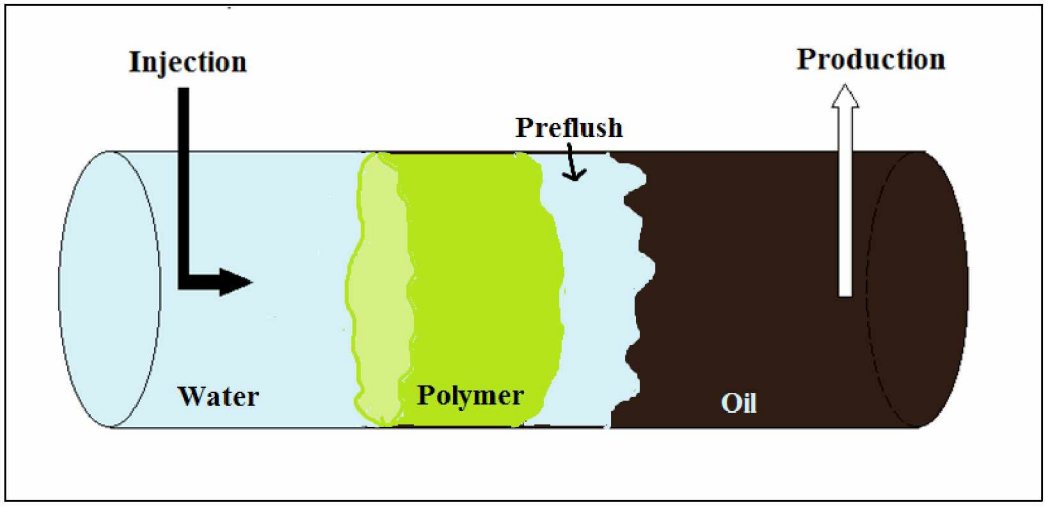

Figure 11: Polymer flooding in heavy oil reservoir

Given the severe mobility difference between the water and the heavy oil, a high molecular weight polymer is added to the injection water. Polymers are very high molecular weight compounds that are made up of long chains of smaller compounds called monomers. In polymer flooding, the polymer reduces the water permeability by mechanical entrapment and enhances the viscosity of the aqueous phase. Polymer flooding has been widely applied as an enhanced oil recovery method in the oil industry to increase the viscosity of flood water to gain mobility control. Flooding polymer gels also improves sweep efficiency by shutting off high permeability thief zones[35]. This characteristic of the polymer solutions can also be useful in shutting off the thief zones in the wormholes produced in CHOPS. Moreover, the use of horizontal injection wells has eased concerns related to the injectivity of polymer solutions[35]. Higher sweep efficiency can result in higher recovery in the long run. All these factors make polymer flooding an attractive EOR method for Ugnu heavy oil reservoirs, with CHOPS being the primary recovery means. Research interests in recent years have been aimed toward evaluating the technical and economic feasibility of polymer flooding.

There are various types of polymers employed for the EOR technique. They are divided into two major categories: synthetic polymers and bio polymers. The most widely used synthetic polymers include synthetic polyacrylamide (PAM) and hydrolyzed polyacrylamide (HPAM) (their chemical structures are shown in Figure 12), and some widely used bio polymers include biological polyacrylamide (which consist of amide monomers), Xanthan gum, carboxy ethoxy hydroxyl ethyl cellulose and more[36].

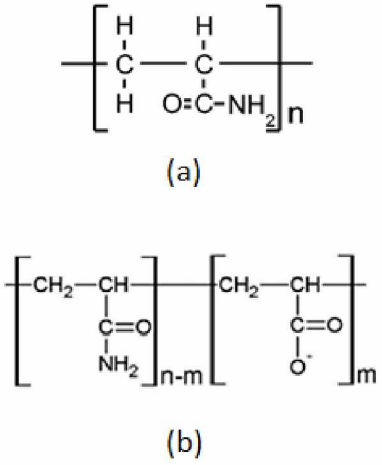

Figure 12: Chemical structures of (a) PAM and (b) HPAM[36]

Hydrolysis helps the polymer dissolve in water, but excess hydrolysis can make the compound sensitive to salinity[37]. Xanthan polymers are biologically generated by dehydrating bacteria[38].

A relatively new type of polymer called an associative polymer is designed to sustain more saline environments. Polymers are also susceptible to degradation under high shear rates, but the shear velocity inside the reservoir in EOR applications is very low, and therefore the shear effects on viscosity are negligible[38].

CHAPTER 3 MODEL CONSTRUCTION AND VALIDATION

3.1 Available Data

To demonstrate the technical viability of heavy oil production from the North Slope, BP started a four-well pilot project in 2011. Due to the limitation of surface location, two horizontal wells (MPS-41A and MPS-39) were selected for appraisal of the Ugnu formation and were installed with surface-driven PCP. In the limited period of production, both the wells produced around 20% of sand cut with oil rates higher than theoretically calculated from the given horizontal sections. Production of MPS-41A is shown in Figure 13.

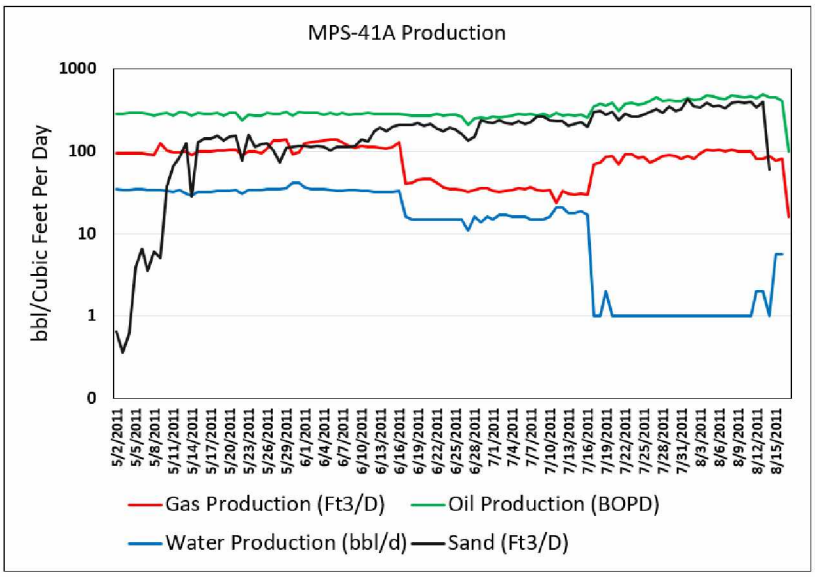

Figure 13: MPS-41A oil, gas, water and sand production[39]

BP started scaling back its heavy oil projects due to significant technological and investment challenges in 2012, and eventually the CHOPS pilot project area was acquired by Hilcorp Ltd. for further development. CHOPS and the subsequent EOR techniques require extensive research before the production activities can be resumed in the project area.

A detailed reservoir fluid study was conducted on the bottomhole oil sample collected from well MPS-41A. The PVT cell was charged with live oil and a Constant Composition Expansion test was performed on the oil. Oil density, oil formation volume factor and gas oil ratio were derived from differentially liberated oil below bubble point pressure. The gas gravities, gas formation volume factor, gas deviation factor and gas expansion factor were determined from differentially liberated gas. The live oil viscosity at reservoir temperature and pressure was measured to be of the order of 5,800 cp. Table 1 summarizes the PVT lab results and Table 2 provides the complete compositional analysis of the oil sample.

Table 1: Summary of PVT laboratory test results for bottomhole fluid sample[39]

Initial Reservoir Conditions		
Reservoir Pressure	1626 psia	11.21 MPa
Reservoir Temperature	71.6 F	295.15 K
Constant Composition Expansion at 71.6 F (295.2 K)		
Saturation Pressure	1390 psi	9.58 MPa
Compressibility at Reservoir Pressure	2.45312E-06 $psia^{-1}$	3.557958E-04 MPa^{-1}
Compressibility at Saturation Pressure	3.64396E-06 $psia^{-1}$	5.285126E-04 Mpa^{-1}
Differential Liberation at 71.6 F (295.2 K)		
At Saturation Pressure		
Oil Formation Volume Factor (Oil FVF)	1.0511 res. Bbl/STB	1.0511 res.m^3/m^3
Solution Gas Oil Ratio (GOR)	116.26 scf/STB	20.71 m^3/m^3
Oil Density	0.9536 g/cm^3	953.6 kg/m^3
Oil Viscosity	5260 cp	5260.0 mPa.s
At Ambient Pressure		
Residual Oil Density	0.9768 g/cm^3	976.8 kg/m3
Residual Oil Viscosity	17753 cp	17753.0 mPa.s
At Tank Conditions		
Residual Oil Density	0.9844 g/cm^3	984.4 kg/m^3
API Gravity	12.24	12.24
Single-stage Separator Test		
At Saturation Pressure		
Oil FVF	1.0497 res. Bbl/STB	1.049 res.m^3/m^3
Solution GOR	114.96 scf/STB	20.47 m^3/m^3
At Tank Conditions		
Residual Oil Density	0.9836 g/cm^3	9833.6 kg/m^3
API Gravity	12.36	12.36

Table 2: Reservoir fluid composition[39]

Boiling Point (F)			Mole Fraction	Mass Fraction	Calculated Properties	
-320.4	Nitrogen	N2	0.0166	0.0010		
-109.3	Carbon Dioxide	CO2	0.0004	0.0000	Total Sample	
-76.6	Hydrogen Sulfide	H2S	0.0000	0.0000		
-259.1	Methane	C1	0.2617	0.0132	Mol. Wt.	318.58
-128.0	Ethane	C2	0.0021	0.0002		
-44.0	Propane	C3	0.0000	0.0000	C6+ Frac.	433.47
10.9	i-Butane	i-C4	0.0000	0.0000	Mol Frac	0.7243
30.9	n-Butane	n-C4	0.0000	0.0000		
82.0	i-Pentane	i-C5	0.0000	0.0000	C7+ Frac	
97.0	n-Pentane	n-C5	0.0000	0.0000	Mol. Wt.	433.49
97-156	Hexanes	C6	0.0000	0.0000	Mol Frac	0.7243
156-208.9	Heptanes	C7	0.0001	0.0000		
208.9-258.1	Octanes	C8	0.0006	0.0002	C12+ Frac	
258.1-303.1	Nonanes	C9	0.0002	0.0001	Mol. Wt.	437.62
303.1-345	Decanes	C10	0.0016	0.0007	Mol. Frac.	0.7143
345-385	Undecanes	C11	0.0067	0.0031		
385-419	Dodecanes	C12	0.0139	0.0070		
419-455	Tridecanes	C13	0.0243	0.0134		
455-486	Tetradecanes	C14	0.0359	0.0214		
486-519.1	Pentadecanes	C15	0.0283	0.0183		
519.1-550	Hexadecanes	C16	0.0292	0.0203		
550-557	Heptadecanes	C17	0.0284	0.0211		
557-603	Octadecane	C18	0.0329	0.0259		
603-626	Nonadecanes	C19	0.0356	0.0294		
626-651.9	Eicosanes	C20	0.0353	0.0304		
651.9-675	Heneicosanes	C21	0.0307	0.0280		
675-696.9	Docosanes	C22	0.0284	0.0272		
696.9-716	Tricosanes	C23	0.0240	0.0240		
716-736	Tetracosanes	C24	0.0249	0.0259		
736-755.1	Pentacosanes	C25	0.0252	0.0273		
755.1-774	Hexacosanes	C26	0.0215	0.0242		
774.1-792	Heptacosanes	C27	0.0199	0.0234		
792.1-809.1	Octacosanes	C28	0.0202	0.0246		
809.1-826	Nanocosanes	C29	0.0189	0.0239		
Above 826	Tricontanes Plus	C30+	0.2367	0.5654		
120.0	Cyclopentane	C5H10	0.0000	0.0000		
162.0	Methylcyclopentane	C6H12	0.0001	0.0000		
178.0	Cyclohexane	C6H12	0.0000	0.0000		
214.0	Methylcyclohexane	C7H14	0.0003	0.0001		
176.0	Benzene	C6H6	0.0001	0.0000		
231.1	Toluene	C7H8	0.0000	0.0000		
277-282	Ethylbenzene & p,m-Xylene	C8H10	0.0000	0.0000		
291.9	o-Xylene	C8H10	0.0000	0.0000		
336.0	1,2,4-Trimethylbenzene	C9H12	0.0002	0.0001		
Total			1.0000	1.0000		

Well trajectories for the horizontal wells MPS-41A and MPS-39 were taken from the well report. Both the wells extend into the M80T formation and were completed with a slotted liner in the leg section. The slotted liner length in MPS-41A is 2,800 ft and that in MPS-39 is 1,175 ft (see Figure 14). The well report provides pore pressures at different formation layers encountered during drilling. The initial reservoir pressure at the top of M80T layer was 1,626 psi. The water saturation along the reservoir depth of Ugnu sands is shown in Figure 15.

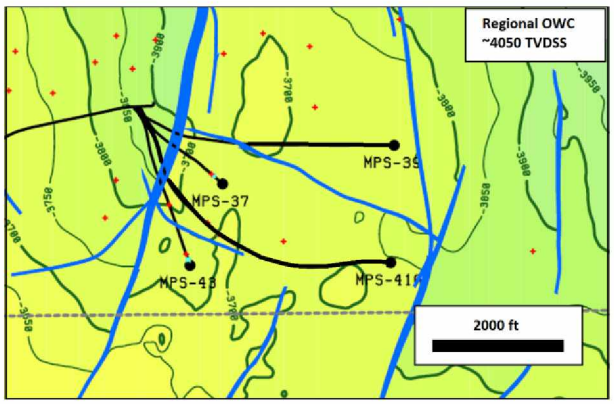

Figure 14: Depth contour map of M80T reservoir sand[2]

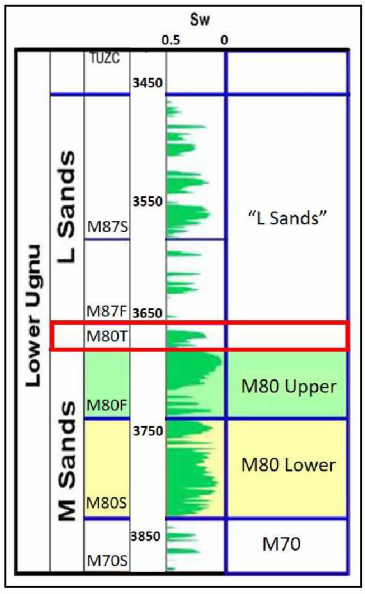

Figure 15: Water saturation along the reservoir depth of Ugnu sands[2]

3.2 Model Construction

3.2.1 Fluid Model Construction

Ugnu reservoirs hold the most viscous oils among the North Slope reserves. MPS-41A produced oil with a live oil viscosity of 5,800 cp. As shown in Figures 16- 21, the native fluid properties were matched by regressing the model-predicted fluid properties using PR EOS with the experimental data. To reduce the simulation time and required system memory, the C7+ fractions were split into 200 pseudo components and then lumped into six hypothetical components of equivalent PVT properties. Regression is the process of tuning the EOS parameters to obtain improved matches between the calculated EOS and the experimental data. Since the pseudo-components are a mixture of multiple individual hydrocarbon components, their critical properties may not have been accurately determined, and thus the pseudo-components were the ideal candidates for regression for tuning the EOS. Saturation pressure of 1,390 psi was matched by tuning the binary interaction coefficient of PR EOS. The average normal boiling points and specific gravities of the C7+ fractions were matched by tuning the Watson characterization factor. Volumetric properties like gas-oil ratio, compressibility factors and formation volume factors were matched by tuning the critical temperature and pressure of the components. Lohrenz Bray Clark[40] viscosity correlation and critical volume were used to match the reservoir fluid viscosity.

Foamy oil was modeled by adding a simple non-equilibrium reaction (Equation 8) available in CMG-STAR that converted CH_4 into a pseudo component named "bubble," preventing it from transforming into a continuous gas phase.

$$CH_4 \rightarrow bubble \tag{8}$$

The critical properties of the bubble component were set to be the same as those of methane. The reaction rate was tuned and set to 2.88E-7 moles/day/ft^3 to match the production history.

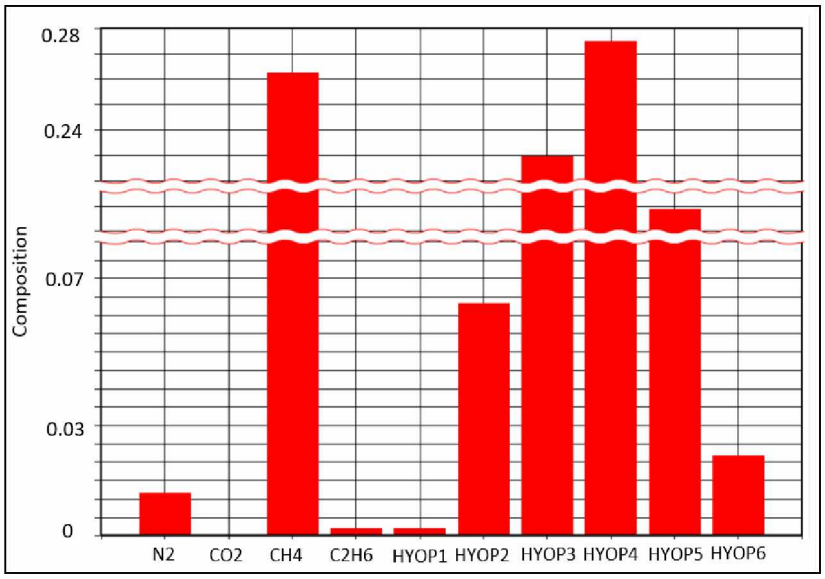

Figure 16: Composition of fluid model

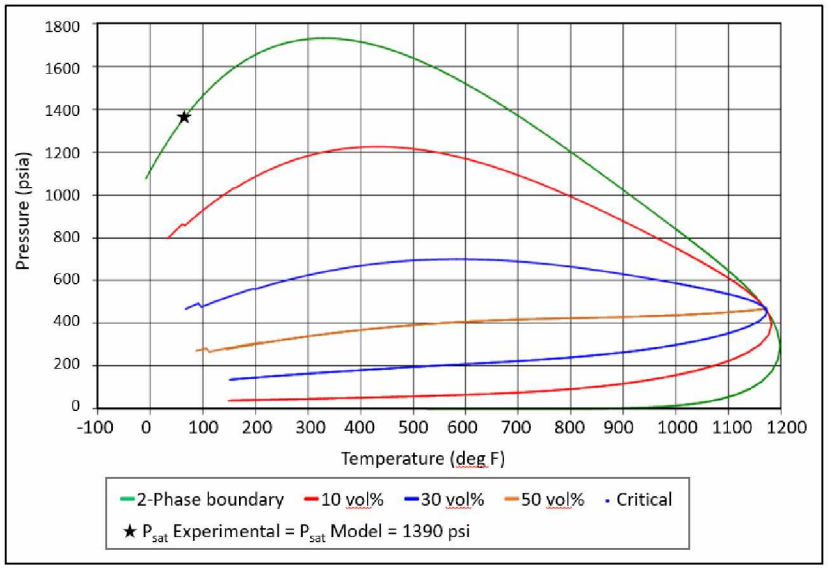

Figure 17: Two-phase envelope generated by EOS

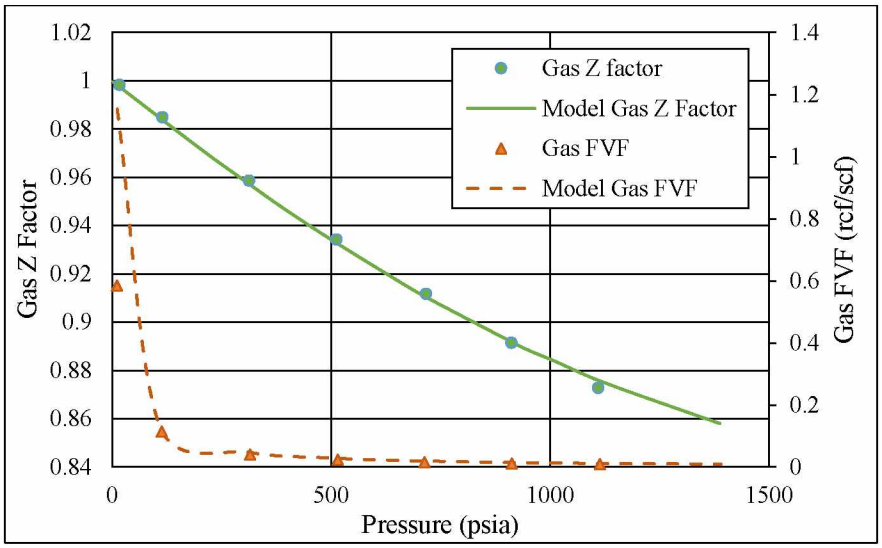

Figure 18: Experimental and model gas compressibility factors (z) and gas formation volume factors (FVF)

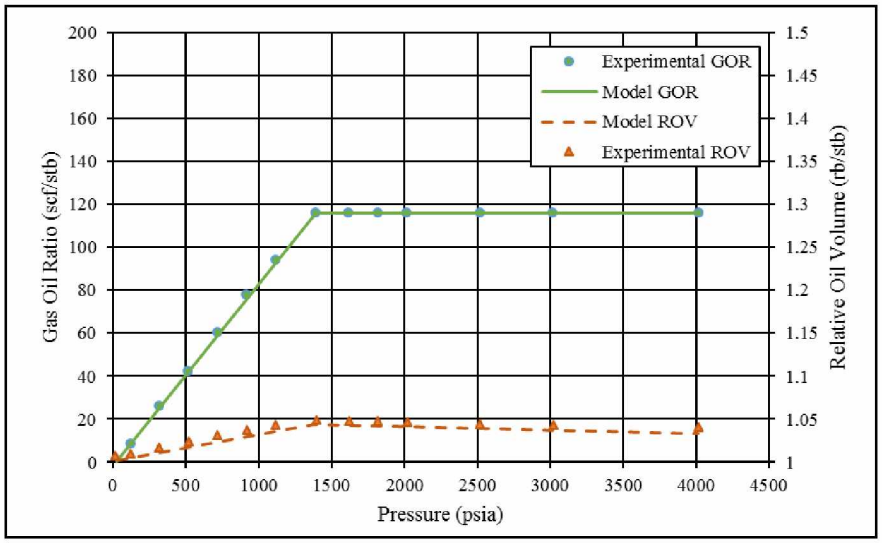

Figure 19: Experimental and model gas oil ratio (GOR) and relative oil volume (ROV)

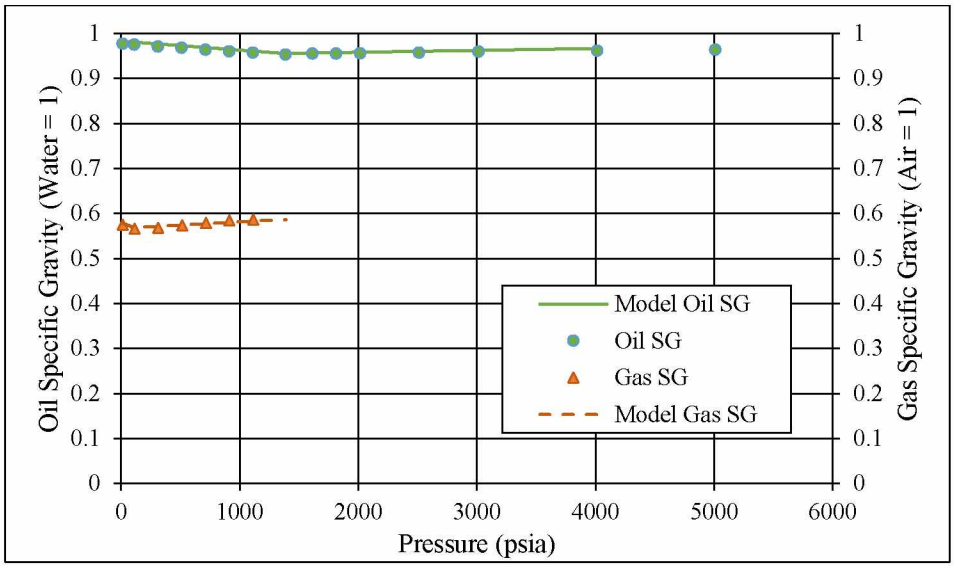

Figure 20: Experimental and model oil and gas specific gravities (SG)

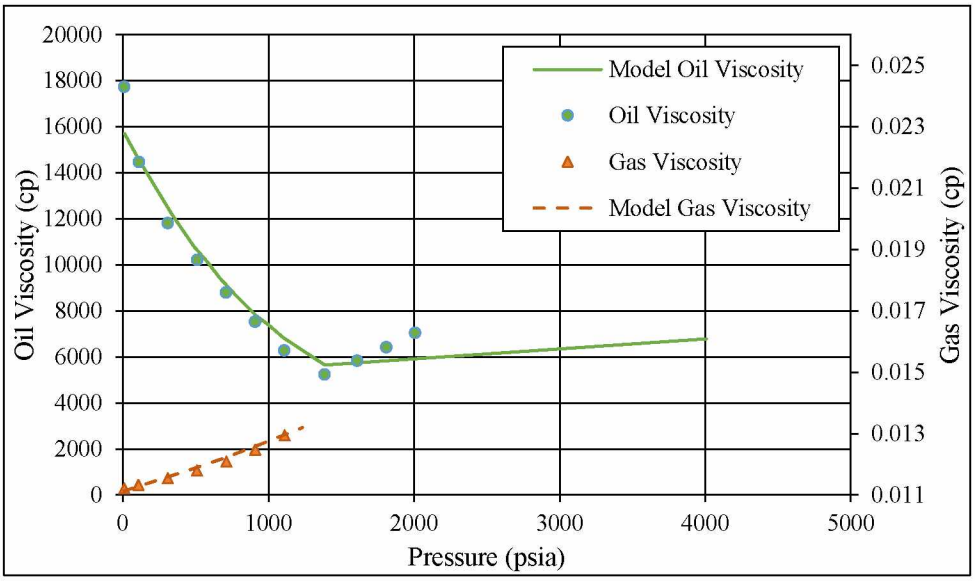

Figure 21: Experimental and model oil and gas viscosities

3.2.2 Reservoir Model Construction

The first step toward building the reservoir model was to digitize the depth contour map for the reservoir sand. This was done using an online plot digitizer. The digitized map of the M80T layer was then imported into the CMG-builder for visualization. The reservoir geometry thus created was then superimposed by a grid structure. Well trajectories for the wells MPS-41A and MPS-39, which were obtained from the well reports[41], were added to the reservoir. To visualize the reservoir in 3D and to simulate the model, a mesh system was required. An orthogonal corner point grid type was selected for this purpose. A 2,000' × 2,200' grid section was placed over the reservoir section in the horizontal i-j plane with 100 grid blocks in each direction. The grid contained the horizontal legs of both the wells that were spread almost parallel to each other in the reservoir (M80T) layer. The vertical extent (k) of the grid section was fixed at 120 ft to accommodate the depths of the two wells (MPS-41A and MPS-39) with 12 layers of 10 ft thickness each. Porosity of the entire grid section was set to 20.56% as calculated from the density log value obtained from the MPS-41A well report[41]. Reservoir permeability was set to 2,500 mD as used in the CHOPS simulation by Shokri et al[27]. Figure 22 shows the resulting grid view of reservoir section with the wells in place. The water saturation data was digitized from the available log[2] and was supplied to the simulator for all different layers of the reservoir model as shown in Figure 23 and Figure 24.

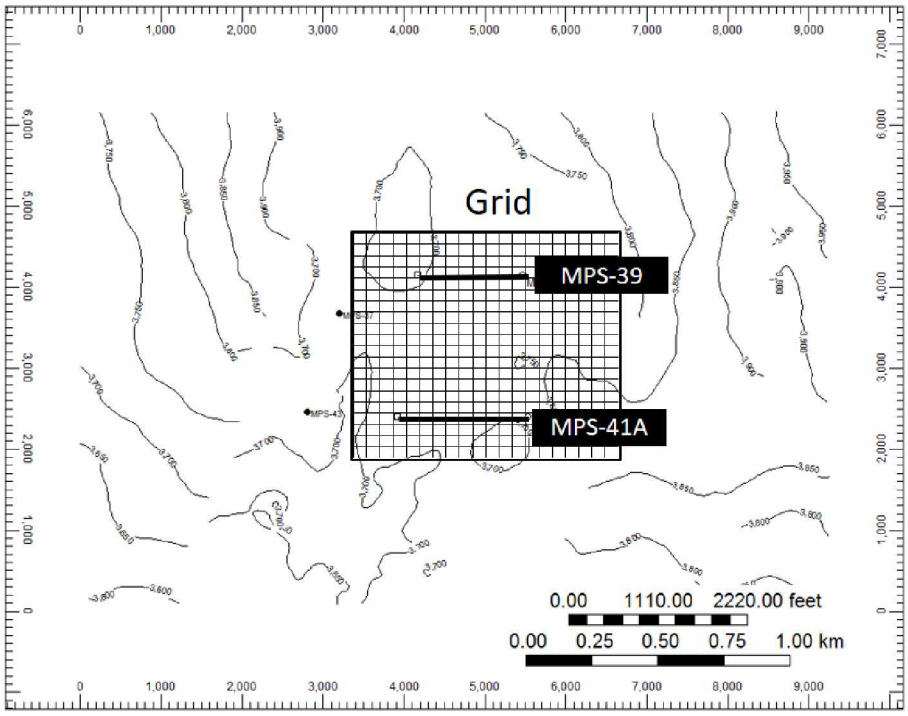

Figure 22: Digitized depth contour map with well trajectories and model grid

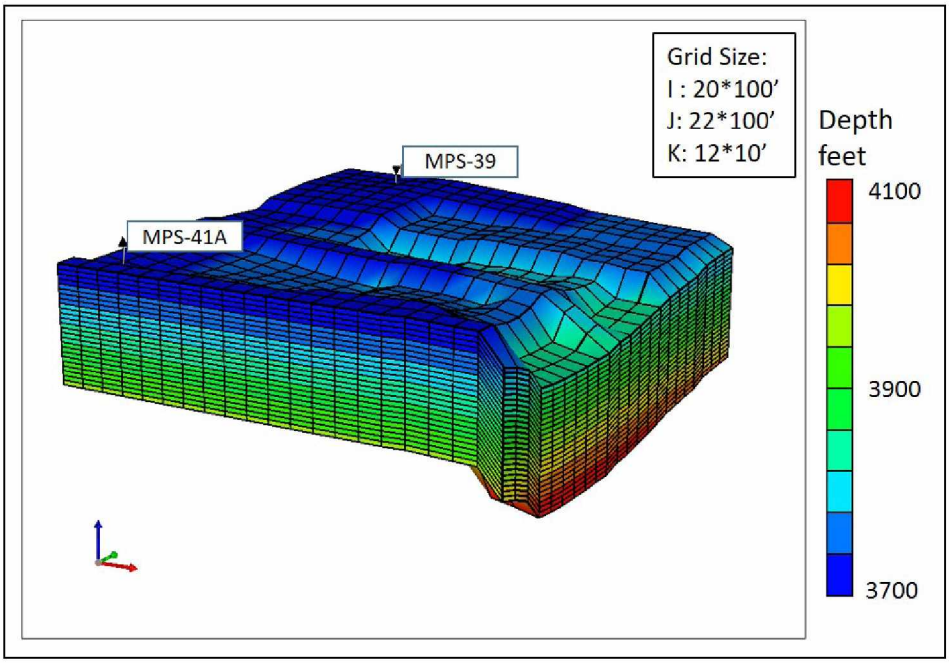

Figure 23: Reservoir model

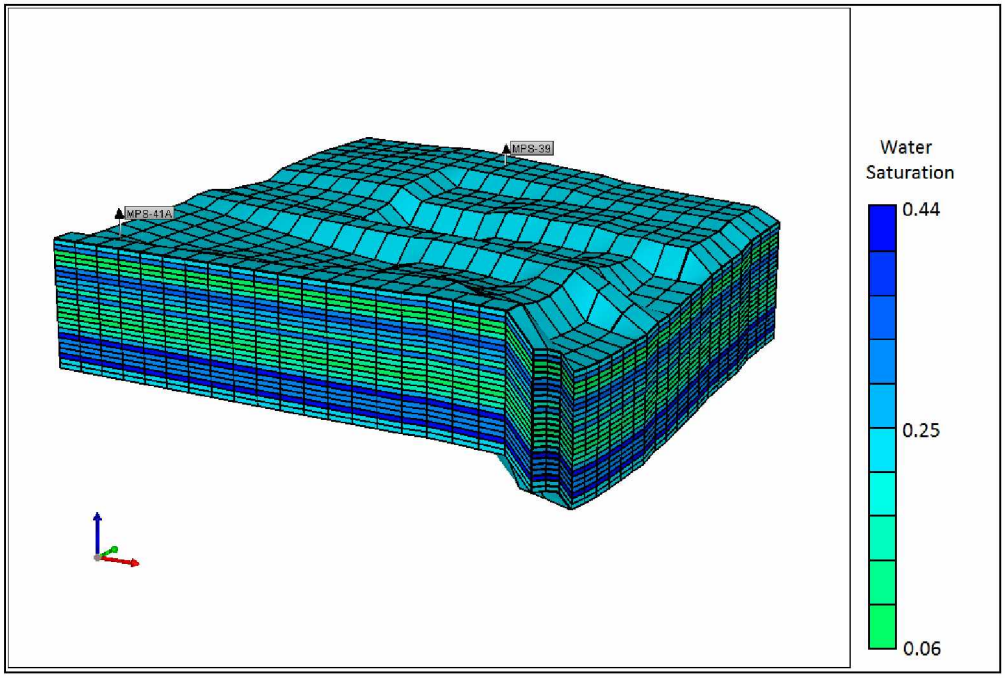

Figure 24: Water saturation variation in the reservoir model layers

3.2.2.1 Wormhole Pattern Generation

Since the areal heterogeneity for the mechanical strength of the rock matrix was not available, the wormhole network pattern in this study was generated using probabilistic modeling. The wormhole is initiated at the perforation. The eight grid blocks surrounding the block containing the perforation were given different random values using the random function in MS Excel. Based on these values, the points of initiation of the wormhole channel or the seed points were decided. Thereafter, new random values were assigned to the seed points and, based on the values, the next step of the wormhole growth was determined, as is shown in Figure 25. The random pattern thus obtained was used to alter the porosity and permeability of the grid blocks that represented the wormhole channel. The altered porosity was set to 60%[42].

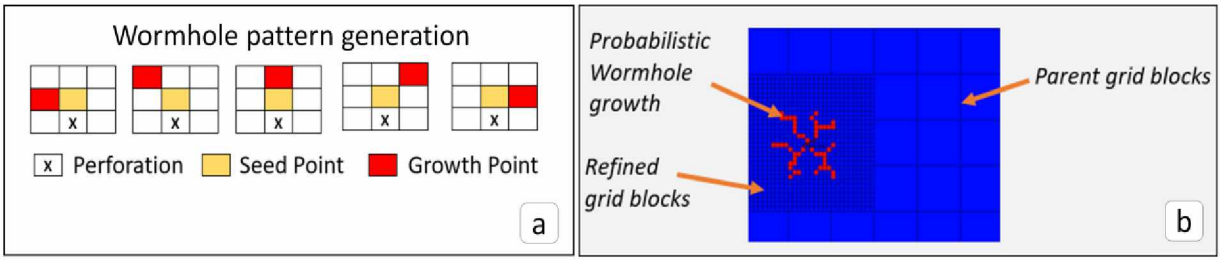

Figure 25: (a) Wormhole pattern generation scheme; (b) Wormhole growth around the perforation within the refined grid system

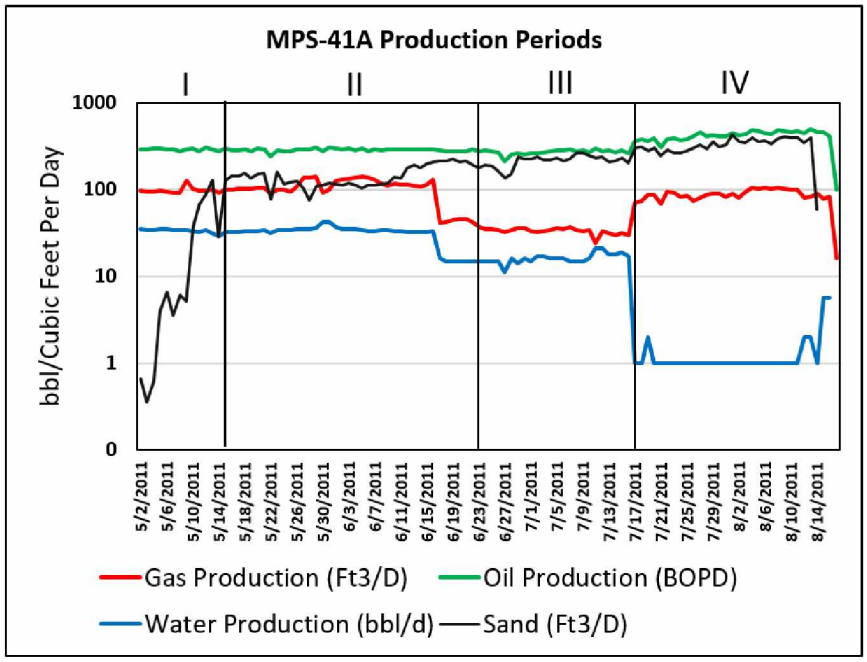

Figure 26: Four simulation periods for MPS-41A CHOPS production

To employ the wormhole pattern into the reservoir model, the grid blocks near wellbore were refined in size. The refined grid blocks had the dimensions of 10' × 10' ×1'. A 39.41% change in porosity in the refined grid blocks that represented the wormhole channel, corresponded to 39.41 ft^3 of sand removal from each block. As the wormhole channel propagates with the production, it was important to input the wormhole pattern in steps. Therefore, as shown in Figure 26, the sand production from the well was divided into four time periods. The extent of the wormhole channel

growth was determined by the sand produced in each period. More precisely, the number of grid blocks to be converted into a wormhole were equivalent to the amount of sand produced for the given time. Figure 27 shows the refined grids and the high porosity gridblocks representing wormholes around the well trajectory.

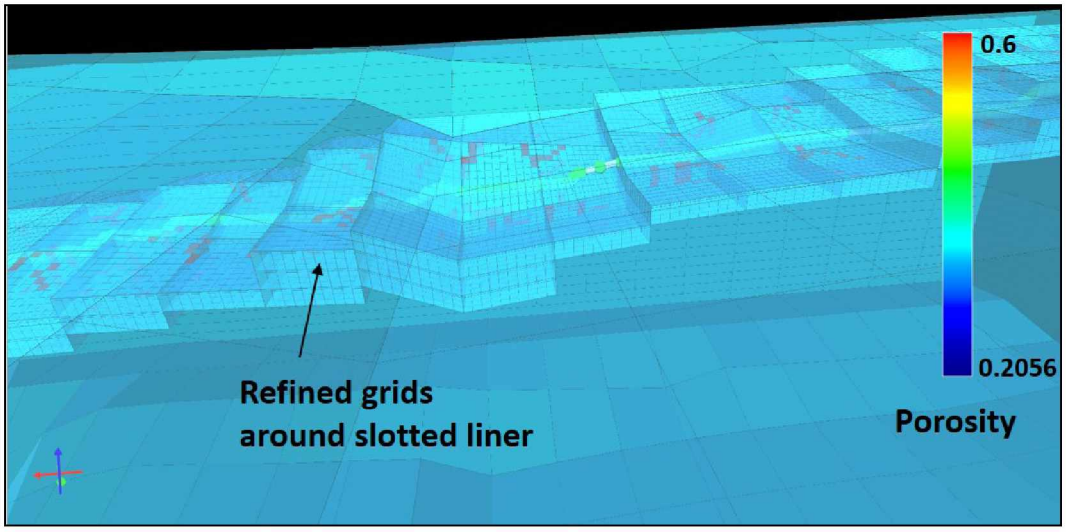

Figure 27: Refined grid system and wormhole pattern around slotted liner completion of MPS-41A

3.3 Model Initialization and Validation

The reservoir model was initialized with an average reservoir pressure of 1,626 psi at datum depth of 3,752 ft TVD from the data available in the well report[41]. Since the bottomhole pressure (BHP) or drawdown data was not available for MPS-4A, a BHP of 125 psi was employed as done in an analogous well MPS-37[43]. This value is quite low as compared to the standard BHP values maintained in oil wells but is essential to creating higher drawdown to initiate sand production. The initial relative permeability tables were adopted from Denbina et al.[28] and modified to match the production history (see Figures 28-30).

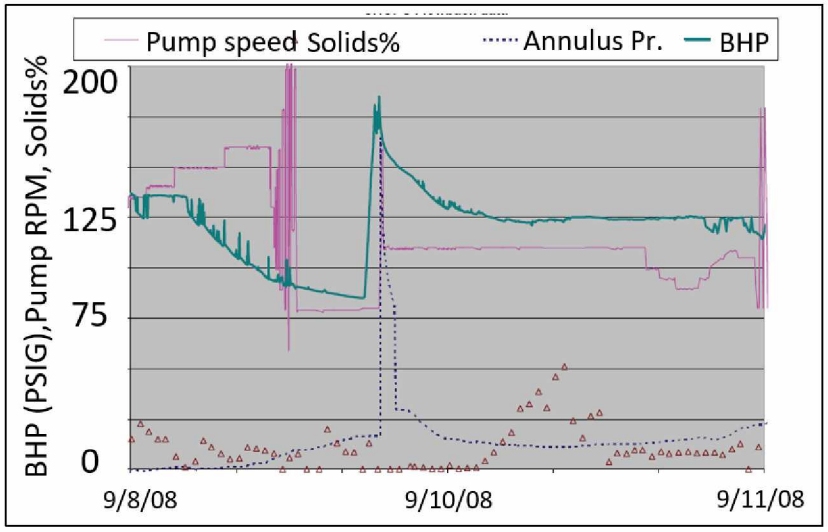

Figure 28: BHP, Pump speed and annulus pressure in MPS-37[43]

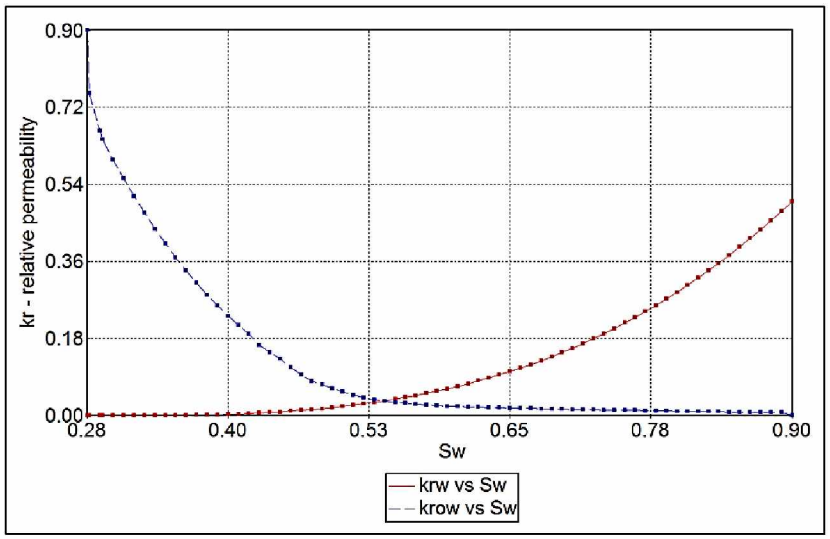

Figure 29: Oil-water relative permeability curves

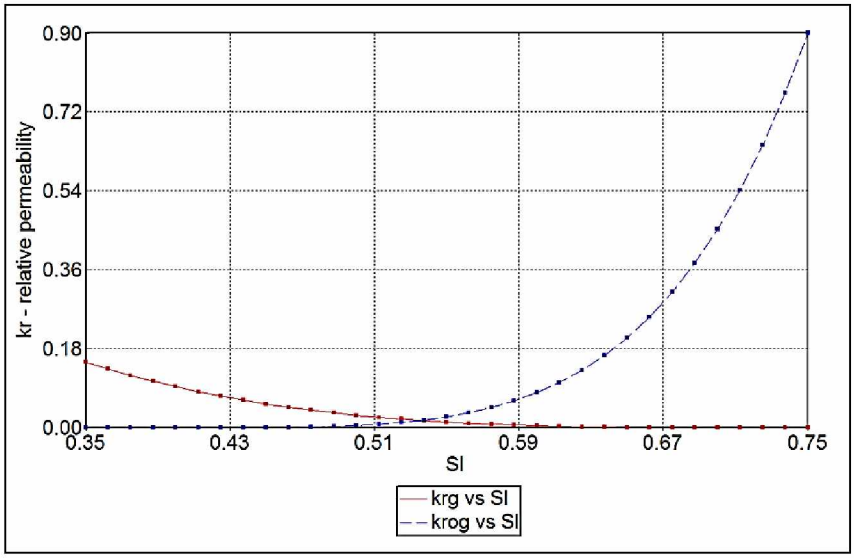

Figure 30: Gas-liquid relative permeability curves

The model was run for the four time periods, as shown in Figure 31. The output reservoir pressures as well as oil, water and gas saturations obtained for all the reservoir grid blocks for a preceding simulation period were used as an input for the subsequent simulation period, thereby maintaining the continuity of the model. The wormhole pattern was updated with each simulation period based on the cumulative sand production.

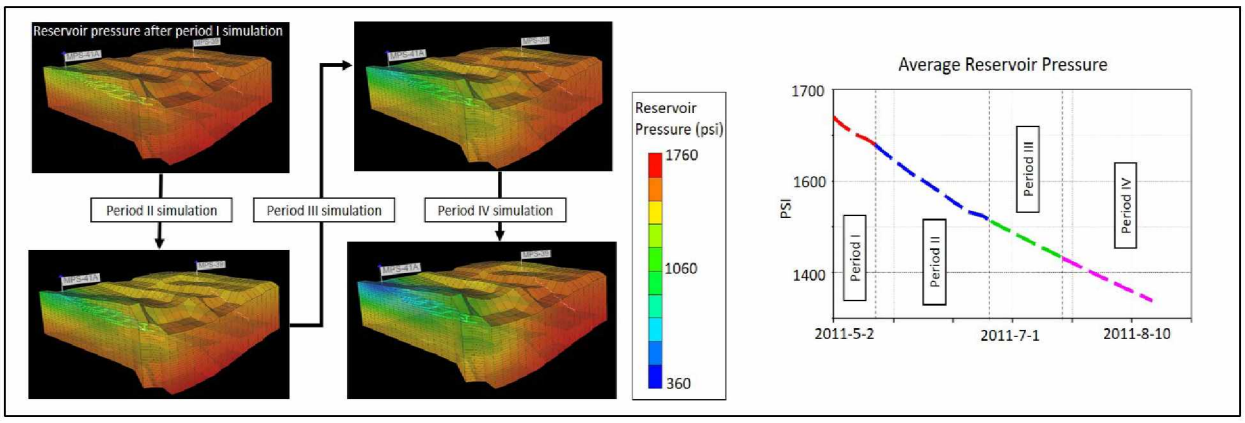

Figure 31: Reservoir pressure after I, II, III and IV period CHOPS simulations and continuity of average reservoir pressure during the simulation

To achieve the best history match, relative permeability, absolute permeability of wormhole channels and non-equilibrium reaction rate were further fine-tuned. The rate of reaction for the non-equilibrium conversion of methane to bubble was set to 2.88E-7 moles/day/ft^3. The absolute permeability of wormholes was increased to 3,500 mD. Gas relative permeability was suppressed to reduce the gas production. Figures 32, 33 and 34 show a reasonable history match between the field production of oil, gas and water matched with the simulation results for MPS-41A.

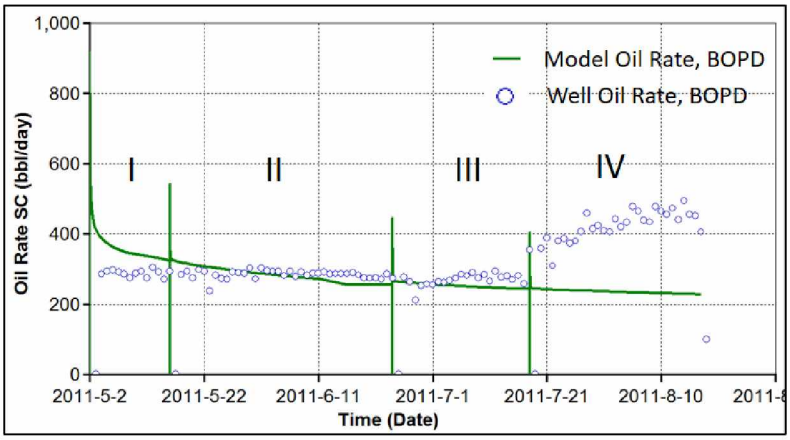

Figure 32: Oil production history match

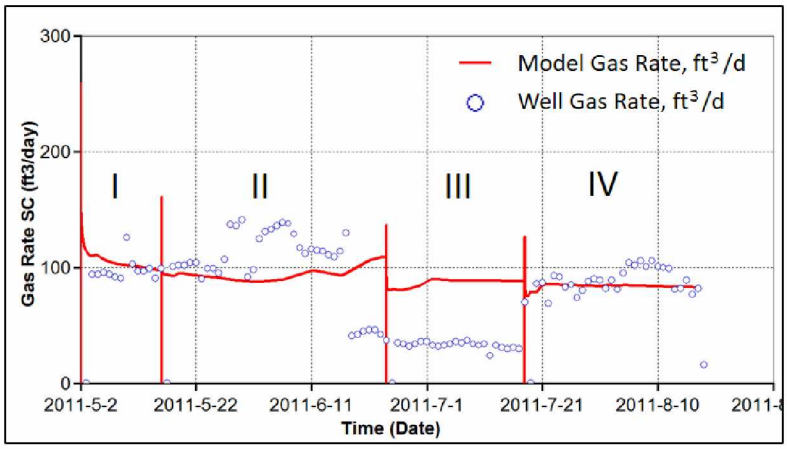

Figure 33: Gas production history match

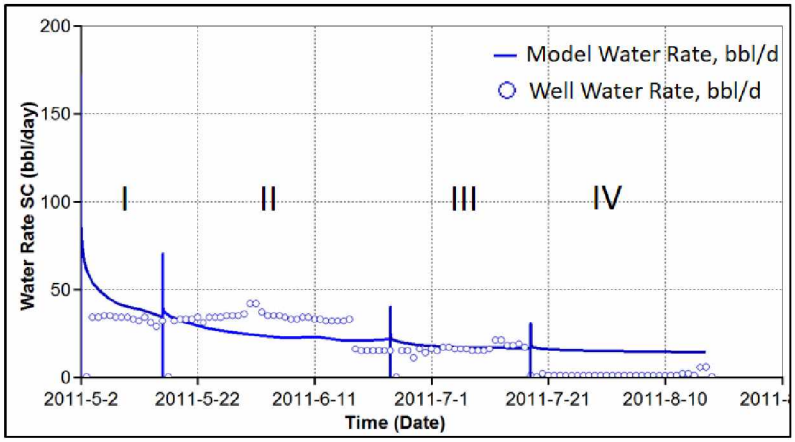

Figure 34: Water production history match

The final reservoir pressures and saturations in each grid block and the final wormhole geometry for each perforation layer obtained after the simulation of period IV were then utilized to carry out a post-CHOPS recovery analysis. A base run on this model for 50 years showed only 1.33% ultimate oil recovery, indicating the need for enhanced recovery solutions. Figure 35 shows the natural depletion on MPS-41A after CHOPS production between the early 2000s and 2032.

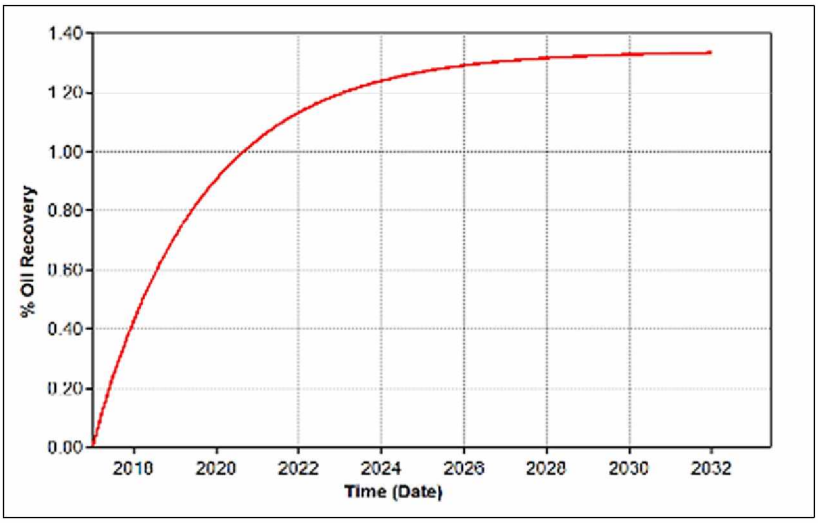

Figure 35: Natural depletion on MPS-41A after CHOPS production

CHAPTER 4 POST-CHOPS RECOVERY OPTIMIZATION

4.1 Water Flooding

Water flooding is carried out in relatively low viscosity reservoirs, like Schrader Bluff, as EOR. The Prince Creek aquifer caters abundant water, which can be utilized for water injection in the Milne Point wells. The aquifer water has low salinity values (Table 3) indicating very low processing costs. Building the infrastructure for transporting the injection water is the main challenge for a new well pad.

Figure 36 depicts the plot of oil recovery factor versus time obtained upon flooding the reservoir with water through the injection well MPS-39 for 50 years. Injection constraints of maximum reservoir pressure of 1,700 psi and maximum injection rate of 5,000 bbl/d were applied. A 50-year simulation of water flooding resulted in a little more than 12% of heavy oil recovery.

The effect of viscous fingering can be observed by analyzing the fractional flow of water inside the reservoir. Higher fractional flow of water indicated a higher bypass of oil in the wormhole channels. Figure 37 depicts the reservoir with transparent grids at different time stages of waterflooding. It can be observed that the fractional flow (f_w) of water near the wormhole zone around the perforations in MPS-41A is higher than the surrounding reservoir. The reservoir layers with higher water saturation experienced earlier breakthroughs of injected water.

Table 3: General water quality parameters of Milne Point Price Creek water wells[44]

Well	pH	Specific Conductivity (mS)	Temperature (°C)	Field Measured Salinity (mg/L)
No. 2	7.85	3.67	18.3	1,800
No. 21	7.69	4.27	19.3	2,100
No. 58	7.74	5.02	18.8	2,600
No. 77	7.73	4.41	18.4	2,200

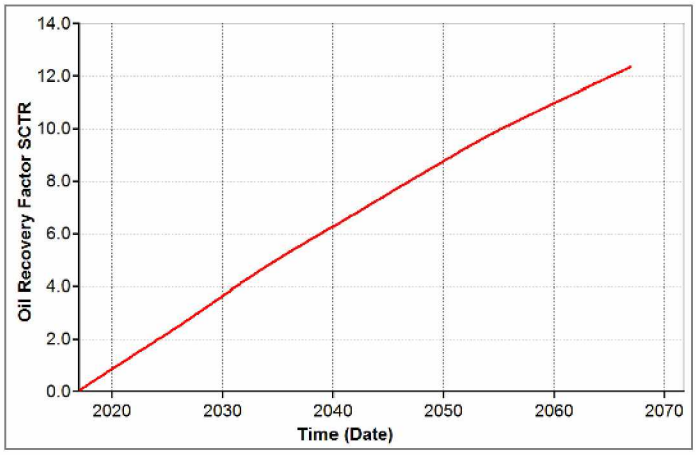

Figure 36: Oil recovery factor with time for 50 years of water flooding

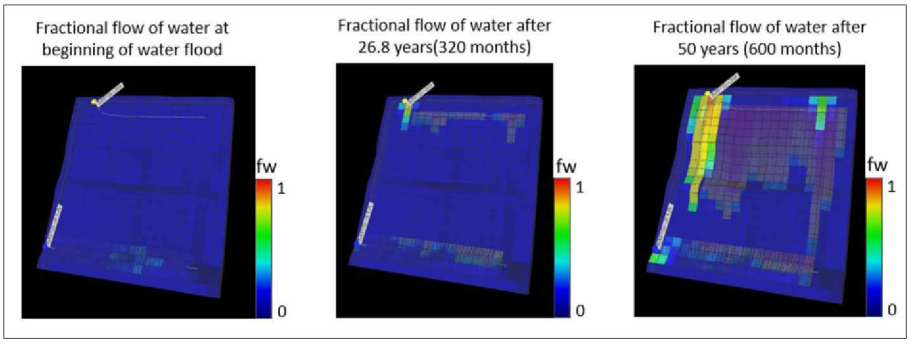

Figure 37: Fractional flow of water inside the reservoir at different stages of water flooding

4.2 Polymer Flooding

4.2.1 Polymer Selection

Table 4 consists of different types of commercially available polymers used for simulation purposes in this study. FP3630 is a conventional polymer, while D11S, S255 and B192 are associative polymers. The associative polymers are designed to be less prone to degradation in a high salinity environment.

Table 4: Technical details of polymers taken from Pancharoen et al.[38].

	FP3630	**D118**	**S255**	**B192**
Molecular weight	Ultra-high	Very high	Medium	Low
Ionic character	Anionic	Anionic	Anionic	Anionic
Charge density	Medium	Medium	Medium	Medium
Approximate bulk density	0.67 kg/m^3	0.8 kg/m^3	0.8 kg/m^3	0.8 kg/m^3
Viscosity measurements	@ 5.0 g/l 1800 cp	@ 5.0 g/l 1700 cp	@ 5.0 g/l 2000 cp	@ 5.0 g/l 2200 cp
	@ 2.5 g/l 700 cp	@ 2.5 g/l 650 cp	@ 2.5 g/l 5500 cp	@ 2.5 g/l 650 cp
	@ 1.0 g/l 260 cp	@ 1.0 g/l 270 cp	@ 1.0 g/l 190 cp	@ 1.0 g/l 140 cp
Dissolution time	90 min	90 min	120 min	120 min

A basic job design was considered to carry out the simulations for polymer selection that included a pre-flush with water for one year, followed by injecting a polymer solution for the next one year, and subsequently followed by water flood to provide a drive to the polymer slug. A preflush of water conditions the reservoir for subsequent EOR. Since the water from the Prince Creek aquifer has very low salinity, a preflush with water from that source will prevent salinity effects on the polymer solution. Well MPS-39 was used as an injection well for this simulation. Injection constraints of maximum reservoir pressure of 1,700 psi and maximum injection rate of 5,000 bbl/d were applied. Figure 38 illustrates a plot between the oil recovery factor versus percentage of pore volumes injected. It is interesting to note that to obtain the same recovery factor, higher pore volumes of water flood were required as compared to the polymer flood.

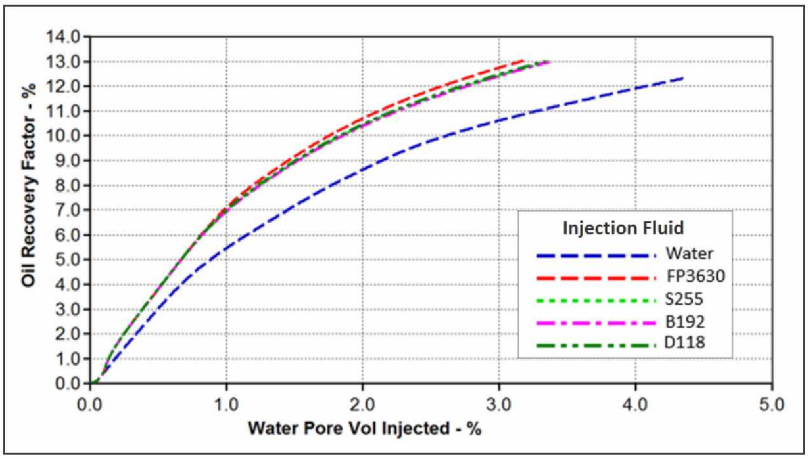

Figure 38: Oil recovery factor versus pore volume of injection for different polymer solutions

The conventional polymer FP3630 showed the marginally highest oil recovery with minimum pore volumes of injection. Since the salinity of the preflush was low enough, FP3630 can be used for the Ugnu reservoir. Therefore, FP3630 was employed for further simulations in this study.

4.2.2 Polymer Concentration Optimization

While narrowing down to the optimum concentration of the polymer in the injection fluid, several factors should be taken into consideration. Besides the overall oil recovery, the injectivity of the solution, reservoir pressure, reservoir fracture pressure and economics should be accounted for during polymer flood design. Simulations using seven different concentrations of the polymer solution were carried out for 50 years (see Figure 39). It was observed that increasing the polymer concentration increased the reservoir pressure rapidly at the beginning of the injection. To prevent fracturing and damage of the reservoir with the injection stream, a safe reservoir pressure should be maintained. With a fracture pressure gradient of approximately 0.58 psi/ft, the upper limit of a safe reservoir pressure for M80T sand was calculated to be 1,750 psi. Thus, a 10,000 ppm polymer solution was selected to be the optimum concentration for polymer flooding at the depth of interest. It was observed that injectivity of polymer solutions after the concentrations 40,000 ppm was negligible. With different fracture pressure and permeability, the optimum polymer concentration can vary. It is also interesting to note that there will be wormhole growth near injection well perforations as well. But, the present work is limited to the wormhole modeling of the production well.

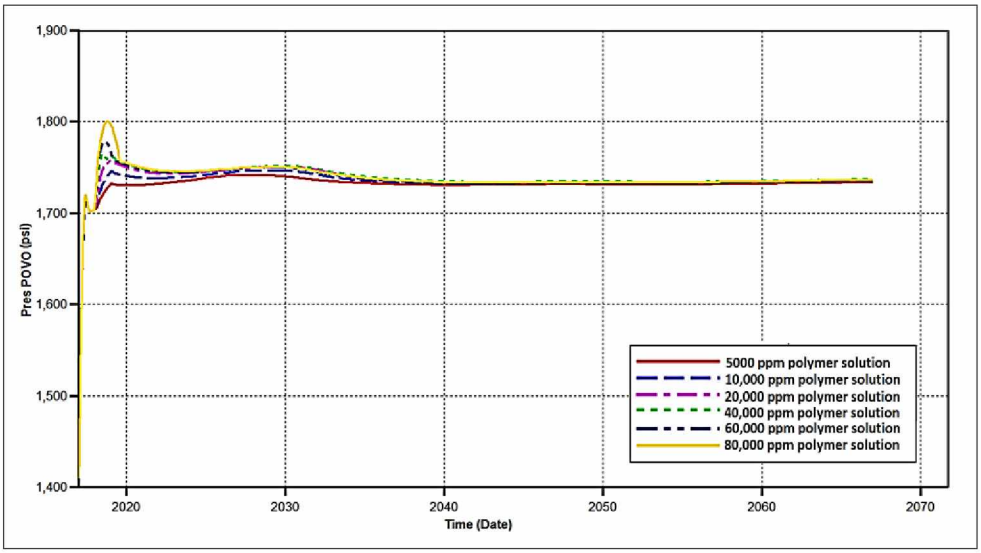

Figure 39: Reservoir pressure vs. time for different concentrations of FP3630 polymer injection

The effect of polymer injection on sweep efficiency can be observed by comparing the fractional flow of the injection fluid during water and polymer flooding at same pore volume of injection. Figure 40 compares the injection water fractional flow in one of the model layers. The viscous fingering effect was observed to be less severe in case of polymer injection as compared to water flooding.

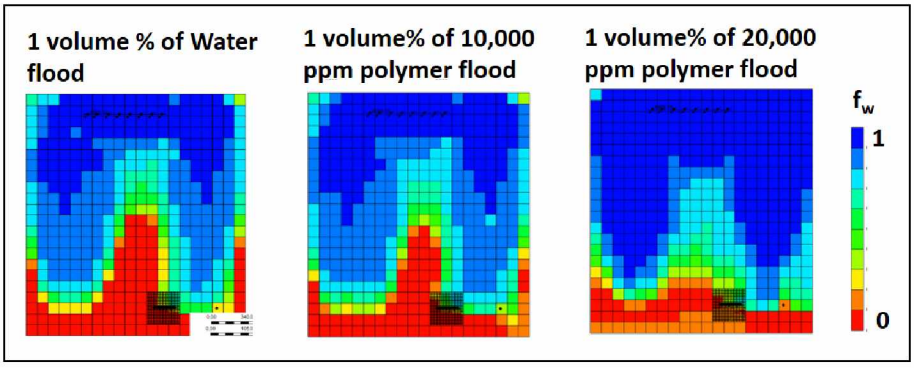

Figure 40: Fractional flow of water at 1 pore volume of water, 10,000 ppm and 20,000 ppm of polymer injection

4.2.3 Injection Time Optimization

Another parameter to be optimized while designing a polymer flood job is the optimum beginning time for injecting the polymer. Three scenarios were simulated depending upon the delay period in injecting the polymer solution: (1) Injection after 1 year of preflush; (2) Injection after 2 years of preflush; and (3) Injection after 5 years of preflush. While the recoveries obtained were similar, the pore volume of injected fluid was least required in case (1). For the initial injection period, the earlier the polymer injection treatment is carried out, the better it is for the overall recovery, as stated by Fabbri et al.[45]. However, after 1% of pore volume injection, it was observed that polymer injection after 5 years yielded higher recovery with less pore volumes of injection (see Figure 41).

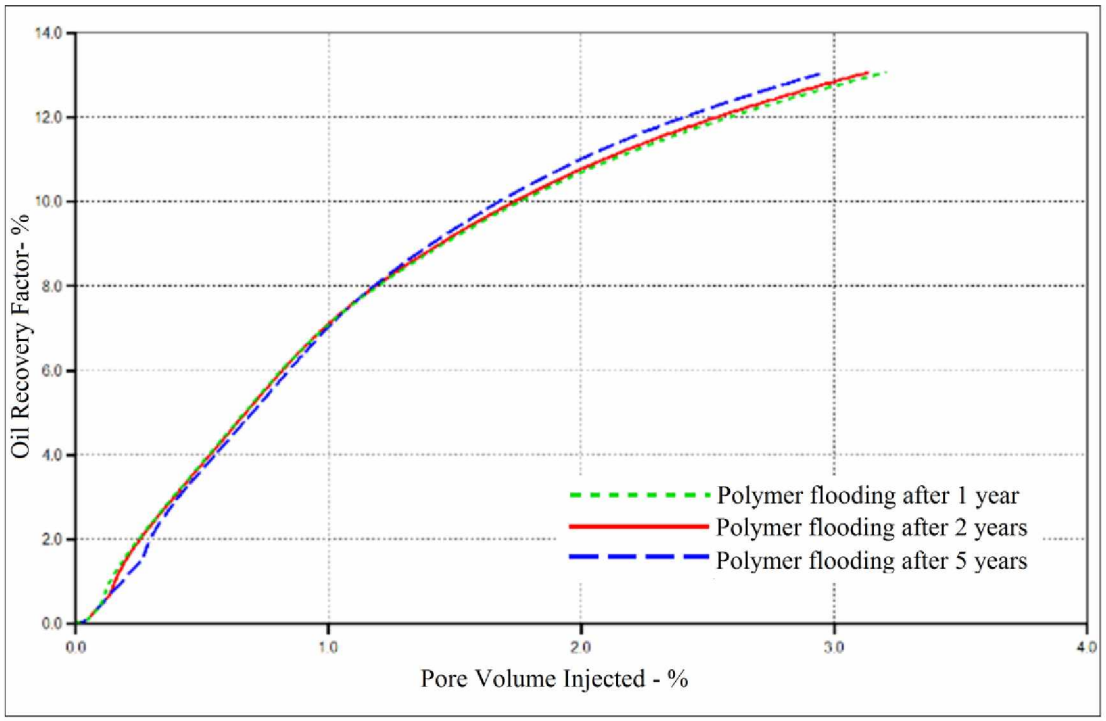

Figure 41: Oil recovery factor for different injection times for 10,000 ppm of FP3630 polymer

4.2.4 Slug Size Optimization

The last step in designing a polymer injection job is determining the slug size. It was observed that oil recovery progressively increased with increment in the slug size (see Figure 42).

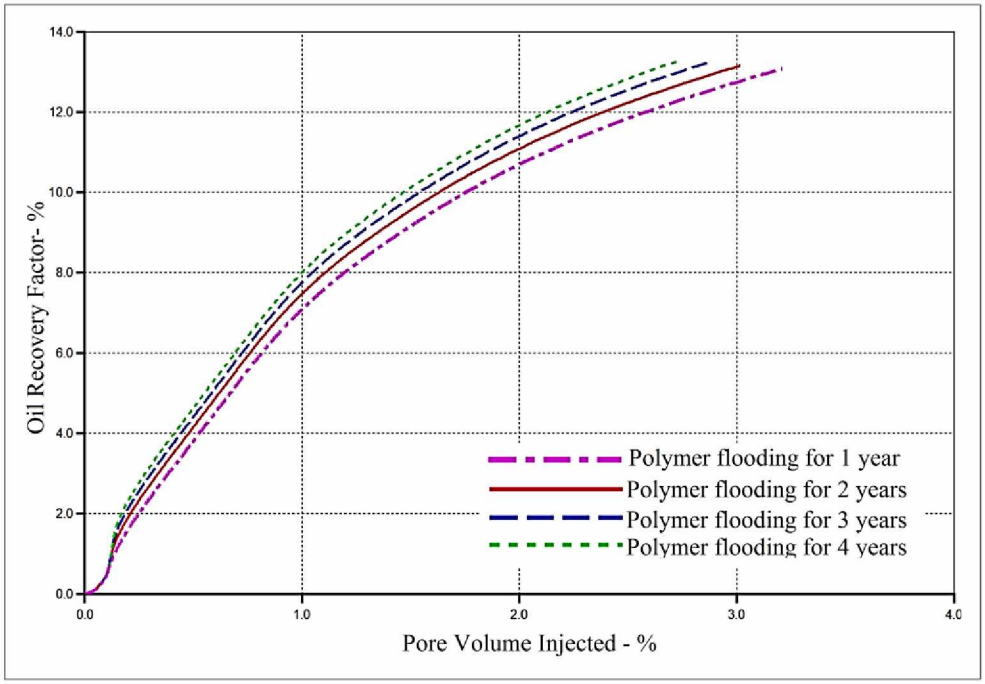

Figure 42: Oil recovery factor for injection of various slug sizes of polymer solution

In this case, an optimum slug size can be determined by an economic evaluation considering the cost of polymer material and procurement, operational costs and oil price.

4.2.5 Well Spacing

Low oil recovery values in the polymer flooding simulations suggest that the spacing between the wells is insufficient for developing the reservoir. The horizontal legs of both the wells are placed approximately 1,700 feet apart. An injection well with same trajectory as MPS-41A was added approximately 1,700 ft from the production well (see Figure 43). Polymer injection was again

carried out with the optimized design and resulted in oil recovery of ~47% after producing from MPS-41A.

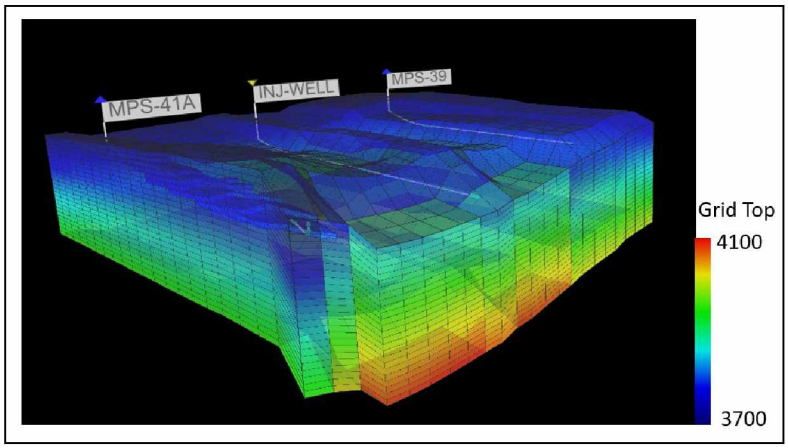

Figure 43: Configuration of MPS-41A, MPS-39 and the new injection well in M80T reservoir

Further investigation was not carried out with this configuration and can be considered for a future research scope. Figure 44 compares the oil recovery values for polymer flooding from the new injection well, polymer flooding from MPS-39 and water flooding from MPS-39.

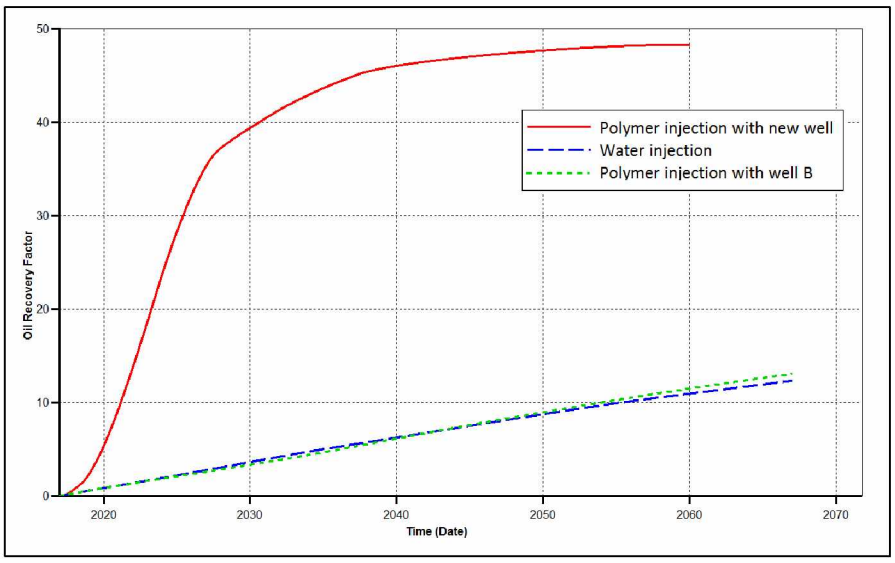

Figure 44: Oil recovery factor for polymer injection from injection well, water injection from MPS-39 and polymer injection from MPS-39

It is evident from the result that the distance between the producing and injecting well significantly affects the overall oil recovery. Moreover, the recovery values obtained in Figure 44 only depict the production from well MPS-41A, while MPS-39 can also be produced simultaneously with the same well configuration.

CHAPTER 5 DISCUSSION OF RESULTS

With its extremely high viscosity, Alaskan shallow depth heavy oil cannot be extracted with natural depletion. The CHOPS method gives us a way to achieve higher recoveries with primary production. But the high porosity channels developed during CHOPS act as bypass routes for high mobility injection fluids, making mobility control an important factor while designing an enhanced oil recovery technique. Since the environmental concerns inhibit thermal recovery, polymer injection appears to be a promising EOR for Ugnu reservoirs. CHOPS production alters the reservoir configuration, which can significantly affect the post-CHOPS reservoir performance. Therefore, a field scale simulation of the CHOPS process and the subsequent EOR can provide a decent idea of the recoveries before the EOR can be implemented. A combination of probabilistic wormhole modeling and foamy oil modeling with a non-equilibrium equation with suppressed gas relative permeability can provide a simple solution to a complicated geo-mechanical phenomenon occurring during CHOPS production. Unlike geo-mechanical modeling, this method does not rely upon extensive reservoir data and requires relatively moderate computational power. The history-matched reservoir model can be used for different EOR simulations.

The conventional polymers like FP3630 can be used for EOR purpose if the low salinity water like from Prince Creek aquifer is utilized as pre-flush. The results obtained for polymer injection study show small improvement in the oil recovery as compared to the water injection. As the viscosity of oil is extremely high, the mobility difference between reservoir fluid and polymer solution remains large resulting in slight improvement in recovery. The concentration of the polymer can only be increased unto the threshold of injectivity and reservoir fracture pressure. Based on the simulations, a 10,000-ppm concentration for polymer solution was

optimum for the reservoir considered in this study. Having these limitations for injection fluid, in-situ oil viscosity reduction can be considered for improving the mobility ratio. Miscible gas injection, alkali and/or surfactant injection are some of the non-thermal viscosity reduction EOR techniques that can be studied for this purpose. Slug size of the polymer solution can be determined with an economic analysis.

To exploit a reservoir with viscosities such as Ugnu, the average number of wells required is always higher than for light oil reservoirs. In support of this argument, the present research indicates that the spacing between the currently drilled horizontal well pair is higher than required. Upon adding a new injection well between the existing wells, provided much higher recovery factor suggesting the need of infill drilling. With limitations of surface access in the ANS region, multilateral wells can be drilled to access more reservoir area.

CHAPTER 6 CONCLUSIONS AND RECOMMENDATIONS

6.1 Conclusions

- Geological modeling of the Ugnu M80T reservoir section was carried out with the help of the CMG-STARS builder using a depth contour map with well placements using the trajectories of the horizontal CHOPS pilot wells MPS-41A and MPS-39.
- Reservoir fluid was accurately modeled in CMG-Winprop and a possible configuration of wormhole growth was generated with the help of a probabilistic approach and employed to the reservoir model.
- The sand production profile indicates that MPS-41A was suspended before the peak sand production was reached, and thus full wormhole growth might not have been reached. Appropriate sand production modeling is required to decide if the pilot wells should continue CHOPS production.
- Extremely low oil recovery values indicate that Ugnu heavy oil is too viscous to produce economical quantities of oil by natural depletion indicating the need for EOR.
- The fractional flow of water in the CHOPS reservoir suggests that wormholes provide a channeling path to the water, trapping the oil in bypassed pockets during water flooding, giving rise to inefficient sweep efficiency.
- Oil recovery factor and sweep efficiency can be increased by combining the conventional water flood EOR with polymer injection. An optimum polymer concentration depends on the porosity and fracture pressure of the reservoir. More than 40,000 ppm polymer concentration results in no injectivity in the reservoir with porosities of the order of ~20%. Thus, reduced injectivity is a key hindrance in application of polymer injection.

- Provided a low salinity of injection water, commercially available polymer FP3630 can be used as a water additive to reduce the viscous fingering with an optimum concentration of 10,000 ppm polymer solution.
- It is better to start the polymer injection earlier during the production life to get higher oil recovery in less pore volumes of polymer injection. However, for a long-term project, the optimization of polymer injection beginning time would vary.
- The well spacing presently used in the Ugnu pilot facility is insufficient to obtain adequate oil recoveries. To optimize well spacing, infill drilling is suggested for the Ugnu reservoir.

6.2 Recommendations

Micro-seismic technology should be developed to dynamically monitor the wormhole growth, which can be used for geo-mechanical model calibration and EOR planning.

Miscible gases can lower the viscosity of heavy oil. Thus, miscibility studies should be conducted for heavy oils from the Ugnu reservoir to determine the optimum gas composition and concentration. Further, surfactants are known to reduce the interfacial tension between oil and water producing an oil-in-water emulsion with significantly lower viscosity than the native reservoir fluid. Heavy oils usually have a high content of organic acids, which can react with alkali to form an in-situ surfactant[46]. The oil-in-water emulsion generated by surfactants can be produced with much ease. It will be worth studying the interfacial interactions of the reservoir fluid with alkali and surfactants to analyze the emulsion formation process. The results of these studies can be used to simulate miscible gas injection and alkali-surfactant flooding in a reservoir that has been produced with CHOPS. As these methods reduce the fluid viscosity, they can also be combined with polymer flooding to take advantage of further improved mobility ratios. Miscible gas-polymer

flooding and alkali-surfactant-polymer flooding combinations can be investigated through experimental and simulation studies for the Ugnu reservoirs.

REFERENCES

1. Dusseault, M. B., Ma, Y., Xu, B., Liang, C. X., & Wu, G. (2002, January 1). *CHOPS in Jilin Province, China*. 79032-MS SPE Conference Paper.
2. Chmielowski J. (2013). *BP Alaska Heavy Oil Production from the Ugnu Fluvial-Deltaic Reservoir*. 2013 Pacific Section AAPG, SEG and SEPM Joint Technical Conference, Monterey, California (2013, April 19-25).
3. Brownbag L. (2011, March). *Heavy Oil vs. Light Oil.* www.aoga.org/wp-content/uploads/2011/03/HRES-3.10.11-Lunch-Learn-BP-Heavy-Oil1.pdf
4. Alvarez, J., Sawatzky, R. P., & Moreno, R. (2014, September 24). *Heavy-Oil Waterflooding: Back to the Future*. Society of Petroleum Engineers. 171090-MS SPE Conference Paper.
5. Hulm, E., Bernaski, G., Kostic, B., Lowe, S., & Matson, R. (2013). Integrated reservoir description of the Ugnu heavy-oil accumulation, North Slope, Alaska, in F. J. Hein, D. Leckie, S. Larter, and J. R. Suter, eds., *Heavy-oil and oil-sand petroleum systems in Alberta and beyond: AAPG Studies in Geology*.
6. Paskvan, F., Turak, J., Jerauld, G., Gould, T., Skinner, R., & Garg, A. (2016, May 23). *Alaskan Viscous Oil: EOR Opportunity, or Waterflood Sand Control First? Society of Petroleum Engineers*. 180463-MS SPE Conference Paper.
7. Werner, P., Piazza, J.-L., & Raiga-Clemenceau, J. (1987, January 1). *Using Dipmeter Data For Enhanced Structural Interpretation From The Seismic. Society of Petrophysicists and Well-Log Analysts*. 1987-II SPWLA Conference Paper.
8. Alaska Journal of Commerce (2015, August).

9. Hallam, R. J., Piekenbrock, E. J., Abou-Sayed, A. S., Garon, A. M., Putnam, T. W., Weggeland, M. C., & Webb, K. J. (1992, September 1). *Resource Description and Development Potential of the Ugnu Reservoir, North Slope, Alaska*. 21779-PA SPE Journal Paper.
10. Han, G., Bruno, M., & Dusseault, M. B. (2007, April 1). *How Much Oil You Can Get From CHOPS. Petroleum Society of Canada*. 07-04-02 PETSOC Journal Paper.
11. Adil, I., & Maini, B. B. (2005, January 1). *Role of Asphaltene in Foamy-Oil Flow*. 94786-MS SPE Conference Paper.
12. Coombe, D., Tremblay, B., Tran, D., & Ma, H. (2001, January 1). *Coupled Hydro-Geomechanical Modelling of the Cold Production Process*. Society of Petroleum Engineers. 69719-MS SPE Conference Paper.
13. Dusseault, M. B. (1993, January 1). *Stress Changes in Thermal Operations*. Society of Petroleum Engineers. 25809-MS SPE Conference Paper.
14. Eastwood, J., & Lebel, P. (1993, January 1). *Analysis of Seismic Images And Reservoir Simulation For Reservoir Monitoring*. Society of Exploration Geophysicists. 1993-1386 SEG Conference Paper.
15. Diaz, E., Prasad, M., Gutierrez, M. A., Dvorkin, J., & Mavko, G. (2001, January 1). *Elastic Properties of Glauconite And Glauconitic Sandstone Reservoirs*. Society of Exploration Geophysicists. 2001-1772 SEG Conference Paper.
16. Trembly, B. (2009, February). Cold Flow: A Multi-Well Cold Production (CHOPS) Model. *Journal of Canadian Petroleum Technology*, Volume 48, No.2.
17. Trembly, B., Sedgwick, G., Forshner, K. (1997, May). Simulation of Cold Production in Heavy-Oil Reservoirs: Wormhole Dynamics. *SPE Reservoir Engineering*, 110-117.

18. Trembly, B., Oldakowski, K. (2003). Modeling of Wormhole Growth in Cold Production. *Transport in Porous Media*, 53, 197-214.

19. Elkins, L.F., Morton, D., & Blackwell, W.A. (1972). *Experimental Fire-flood in a Very Viscous Oil-Unconsolidated Sand Reservoir, S.E. Pauls Valley Field, Oklahoma*. Fall Meeting Society of Petroleum Engineers of AIME, San Antonio, Texas, USA, 8-11 October. SPE-4086-MS Conference Paper.

20. Yeung K. (1995, February 12-17). *Cold Flow Production of Crude Bitumen at the Burnt Lake Project, Northeastern Alberta*. 6th UNITAR International Conference on Heavy and Tar sands, Houston.

21. Smith, G.E. (1986). *Fluid Flow and Sand Production in Heavy Oil Reservoir under Solution Gas Drive*. 56th California Regional Meeting of the Society of Petroleum Engineers, Oakland. SPE-15094 Conference Paper.

22. Loughead, D.J., & Saltuklaroglu, M. (1992). *Lloydminster Heavy Oil Production: Why So Unusual*. 9th Annual Heavy Oil and Oil Sands Technology Symposium, Calgary.

23. Chugh, S., Baker, R., Telesford, A., & Zhang, E. (1997, January 1). *Mainstream Options For Heavy Oil: Part I-Cold Production*. Petroleum Society of Canada. 97-99 PETSOC Conference Paper.

24. Ehlig-Economides, C. A., & Economides, M. J. (2000, January 1). *Single Well Reservoir Management - the Ultimate Multibranch Well Challenge*. Society of Petroleum Engineers. 59447-MS SPE Conference Paper

25. Chen, S., Lines, L., Embleton, J., Daley, P. F., & Mayo, L. (2003, January 1). *Cold Production Footprints of Heavy Oil On Time-lapse Seismology: Lloydminster Field, Alberta*. Society of Exploration Geophysicists. 2003-1438 SEG Conference Paper

26. Dusseault, M., Shand, D., & Davidson, B. (2002, January 1). *Pressure Pulse Workovers in Heavy Oil. Society of Petroleum Engineers*. 79033-MS SPE Conference Paper.

27. Shokri, R.A., & Babadagli, T. (2014, March 1). *Modelling of Cold Heavy-Oil Production with Sand For Subsequent Thermal/Solvent Injection Applications*. Society of Petroleum Engineers. 158934-PA SPE Journal Paper.

28. Denbina, E. S., Baker, R. O., Gegunde, G. G., Klesken, A. J., & Sodero, S. F. (2001, March 1). *Modelling Cold Production for Heavy Oil Reservoirs*. 01-03-01 PETSOC Journal Paper.

29. Denney, D. (1999, September 1). *Wormhole-Network Model of Cold Production in Heavy Oil*. 0999-0102-JPT SPE Journal Paper.

30. Robinson, D. B, & Peng, D. Y., (1978, March). *The Characterization of the Heptanes and Heavier Fractions for the GPA Peng-Robinson Programs*. Gas Processors Association, Research Report RR-28.

31. Kraus, W. P., McCaffrey, W. J., & Byod, G. W. (1993, May 9-12). *Pseudo-Bubble Point Model for Foamy Oils*. CIM 1993 Annual Technical Conference, Calgary. CIM 93-45.

32. Lebel, J. P. (1994, March 2). *Performance Implications of Various Reservoir Access Geometries*. 11th Annual Heavy Oil & Oil Sands Technical Symposium, Calgary.

33. Claridge, E. L., & Prats, M. (1995, June). *A Proposed Model and Mechanism for Anomalous Foamy Heavy Oil Behavior*. 1995 International Heavy Oil Symposium, Calgary. SPE 29243.

34. Geilikman, M.B., Dusseault, M.B. (1999). *Sand Production Caused by Foamy Oil Flow, Transport in Porous Media*; 35: pp. 59-272.

35. Osvaldo, S. (2015). *Theoretical and numerical study of polymer flooding*. Norwegian University of Science and Technology.

36. Lee, K. S. (2009, January 1). *Application of Horizontal Wells for Injection or Production during Polymer Flood Processes*. 127526-MS SPE Conference Paper.

37. Shupe, R. D. (1981, August 1). *Chemical Stability of Polyacrylamide Polymers*. 9299-PA SPE Journal Paper.

38. Pancharoen, M., Thiele, M. R., & Kovscek, A. R. (2010, January 1). *Inaccessible Pore Volume of Associative Polymer Floods*. 129910-MS SPE Conference Paper.

39. Mr. Anthony McConkey of Hilcorp Energy Co., personal communication. Date: 2016, October 4.

40. Lohrenz, J., Bray, B. G., & Clark, C. R. (1964). *Calculating Viscosities of Reservoir Fluids From Their Compositions*. J Pet Technol 16 (10): 1171–1176. SPE-915-PA.

41. Alaska Oil and Gas Conservation Commission's Online Public Databases. MPS-41A Well File Image Database. http://doa.alaska.gov/ogc/publicdb.html. Date accessed: 2016, January 22.

42. Meza-Díaz, B. I., Sawatzky, R., & Kuru, E. (2012, December 1). *Sand on Demand: A Laboratory Investigation on Improving Productivity in Horizontal Wells Under Heavy-Oil Primary Production--Part II*. 133500-PA SPE Journal Paper.

43. Young, J. P., Mathews, W. L., & Hulm, E. (2010, January 1). *Alaskan Heavy Oil: First CHOPS at a vast, untapped arctic resource*. 133592-MS SPE Conference Paper.

44. McGuire, P. L., Chatham, J. R., Paskvan, F. K., Sommer, D. M., & Carini, F. H. (2005, January 1). *Low Salinity Oil Recovery: An Exciting New EOR Opportunity for Alaska's North* Slope. 93903-MS SPE Conference Paper.

45. Fabbri, C., Cottin, C., Jimenez, J., Nguyen, M., Hourcq, S., Bourgeois, M., & Hamon, G. (2014, January 19). *Secondary and Tertiary Polymer Flooding in Extra-Heavy Oil: Reservoir Conditions Measurements - Performance Comparison*. 17703-MS IPTC Conference Paper.

46. Cui, J., & Babadagli, T. (2016, September 26). *Solvent Retrieval During Miscible Flooding in Heterogeneous Reservoirs Using New Generation Nano EOR Materials: Visual Analysis Through Micro Model Experiments*. 181320-MS SPE Conference Paper.

APPENDIX

CMG-Winprop source code for regressed fluid model

```
**FILE NAME:    Ugnu_C7split_regression_complete.dat
*FILENAMES *OUTPUT *SRFOUT *REGLUMPSPLIT *NONE *GEMOUT *NONE
        *STARSKV *NONE *GEMZDEPTH *NONE *IMEXPVT *NONE
*WINPROP    2016.10

**=-=-=Titles/EOS/Units
**REM
*UNIT *FIELD
*INFEED *MOLE
*MODEL *PR *1978

**=-=-=Component Selection/Properties
**REM
*NC 10 10
*TRANSLATION   1
*EXCESSPROP  *EOS

*COMPNAME
'N2'  'CO2'  'CH4'  'C2H6'  'HYP01'
'HYP02'  'HYP03'  'HYP04'  'HYP05'  'HYP06'

*HCFLAG
0  3  1  1  1
1  1  1  1  1

*PCRIT
33.5  72.8  45.4  48.2  29.978185
20.730555  13.331704  8.9031803  6.8061682  5.4192644

*TCRIT
126.2  304.2  190.6  305.4  570.61659
676.5172  807.14166  876.9386  998.04  1125.2102

*AC
0.04  0.225  0.008  0.098  0.29115922
0.48321738  0.79285251  1.1419451  1.3639462  1.5151726

*MW
27.46  44.01  16.069  30.34  103.55183
163.69557  275.99155  449.21055  702.11086  802.76887
```

*VSHIFT
-0.12956512 -0.09434672 -0.15380517 -0.12343648 0.020663275
0.11877325 0.25276083 0.34687877 0.30962407 0.28293822

*VSHIF1
-0.00020275356 -0.0043565324 -0.00063964178 -0.0059093949 -0.00011215359
-0.00014587782 -0.00014659258 -0.00014643777 -0.00014012768 -0.00013345411

*TREFVS
60.0 60.0 60.0 60.0 60.000008
60.000008 60.000008 60.000008 60.000008 60.000008

*ZRA
0.2905 0.2736 0.2876 0.2789 0.26202973
0.24884621 0.23257871 0.22657455 0.22779737 0.19941059

*VCRIT
0.0895 0.094 0.099 0.148 0.41117688
0.6563779 1.093739 1.5876958 1.9802724 2.3008531

*VISVC
0.0895 0.094 0.099 0.148 0.41117688
0.6563779 1.3199648 2.499393 2.7970271 2.3008531

*OMEGA
0.45723553 0.45723553 0.45723553 0.45723553 0.45723553
0.45723553 0.45723553 0.45723553 0.45723553 0.45723553

*OMEGB
0.077796074 0.077796074 0.077796074 0.077796074 0.077796074
0.077796074 0.077796074 0.077796074 0.077796074 0.077796074

*SG
0.809 0.818 0.3 0.356 0.75695868
0.80538288 0.86441313 0.9233533 0.98091517 1.0404246

*TB
-320.35 -109.21 -258.61 -127.57 230.63167
421.01304 679.07992 943.09461 1187.4909 1431.2763

*PCHOR
41.0 78.0 77.0 108.0 299.48186
458.38496 712.47577 995.61181 1171.9068 903.72778

*IGHCOEF
-0.65665 0.254098 -1.6624e-005 1.5302e-008 -3.0995e-012 1.5167e-016 0.048679

```
0.09688  0.158843  -3.3712e-005  1.48105e-007  -9.66203e-011  2.073832e-014  0.151147
-2.83857  0.538285  -0.000211409  3.39276e-007  -1.164322e-010  1.389612e-014  -0.602869
-0.01422  0.264612  -2.4568e-005  2.91402e-007  -1.281033e-010  1.813482e-014  0.083346
0.0  -0.058883628  0.00043637756  -6.7447452e-008  0.0  0.0  0.0
0.0  -0.036380564  0.00041892022  -6.1944707e-008  0.0  0.0  0.0
0.0  -0.018636861  0.00040507056  -5.7542311e-008  0.0  0.0  0.0
0.0  -0.011497465  0.00039801215  -5.56484e-008  0.0  0.0  0.0
0.0  -0.010340992  0.0003923296  -5.4961518e-008  0.0  0.0  0.0
0.0  -0.0092065246  0.00038308697  -5.3981617e-008  0.0  0.0  0.0

*HEATING_VALUES
0.0  0.0  844.29001  1478.46  0.0
0.0  0.0  0.0  0.0  0.0

*IDCOMP
0  0  0  0  0
0  0  0  0  0

*VISCOR  *HZYT
*MIXVC  0.81980606

*VISCOEFF
0.1023  0.023364  0.0374608  -0.048909  0.0193512
*HREFCOR  *HARVEY

*PVC3  1.3688027

*BIN
0.0
0.025  0.105
0.01  0.13
0.1  0.115
0.13  0.09
0.12  0.15
0.12  0.15
0.12  0.15
0.12  0.15

*SALINITY  *WTFRAC  0.0

**=-=-=Composition
**REM
*COMPOSITION  *PRIMARY
0.011633648  0.00040116026  0.2624591  0.0021060914  0.0019213393
0.063170815  0.22944368  0.27470576  0.13229206  0.021866339
```

```
**=-=-=Plus Fraction Splitting_E
**REM
***SPLIT
***OUTPUT 2
***DMODEL  -1
***ICN  7
***LUMP-METHOD  1
***CRITCOR  *TWU
***NSAMPLE  1
***INTERVAL-TYPE  2
***TBCOR  3
***CHARFACT  *WHITSON
***CHARMULT  1.0
***MINTERVAL  14.026
***ZEND  0.95
***BIAS  0.75
***MINRESVAL  3
***MINRESTYPE  1
***MINFRACS  1
***SAMPLE  'Sample 1'
***MWPLUS  433.49
***SGPLUS  0.93
***ZPLUS  0.7243
***SCN-GROUPS  200
***MUDCLEAN  0
****NUM_OF_FRACTIONS    24
****NUM_OF_COLUMNS    4
***ANALYSIS
**    0.0001  96.0
**    0.0006  106.1933333
**    0.0002  121.0
**    0.0016  139.37875
**    0.0067  147.4026866
**    0.0139  160.4359712
**    0.0243  175.6778601
**    0.0359  189.9056267
**    0.0283  206.0075618
**    0.0292  221.4785616
**    0.0284  236.6914789
**    0.0329  250.7970213
**    0.0356  263.0969663
**    0.0353  274.357847
**    0.0307  290.5615635
**    0.0284  305.1188732
**    0.024  318.58
**    0.0249  331.3743775
```

```
**    0.0252  345.1283333
**    0.0215  358.5877209
**    0.0199  374.6116583
**    0.0202  387.9736634
**    0.0189  402.8604233
**    0.2367  760.9849261

**=-=-=Two-phase Envelope_E
***ENVELOPE
***LABEL    'Before regression'
***FEED  *MIXED 1.0
***KVALUE  *INTERNAL
***OUTPUT 1
***STABCHECK *YES
***TRACEBOTH *NO
***X-AXIS     *TEMP
***RANGT     -148.0    1292.0
***Y-AXIS     *PRES
***RANGP     0.0    14695.95
***PRES    14.69595
***TEMP    1000.0
***MAXSP   99
***STEPDIR   0.2
***RANGFV    -10.0    10.0
***NTAB   0
***NQUALITY    4
***QUALITY
**0.0   0.1   0.3   0.5

**=-=-=Regression Parameters_E
**REM
***REGRESSION
***NTOTREGP  14
***CONVTOL  1.0e-006
***MAXIT  99
***NREGPAR  5
***GROUPCTRL  *INCR
***VIS-EXP
***LOWER-B    0.64
***UPPER-B    1.44
***VIS-COEMU    1
***LOWER-B    0.0523776
***UPPER-B    0.14731
***VIS-COEMU    2
***LOWER-B    0.0119624
***UPPER-B    0.033643
```

***VIS-COEMU 3
***LOWER-B 0.0374608
***UPPER-B 0.10114
***VIS-COEMU 4
***LOWER-B -0.048909
***UPPER-B -0.0366822
***VIS-COEMU 5
***LOWER-B 0.0074659
***UPPER-B 0.0193512
***VIS-VCMU 5
***LOWER-B 0.32894
***UPPER-B 0.71051
***VIS-VCMU 6
***LOWER-B 0.5251
***UPPER-B 1.1342
***VIS-VCMU 7
***LOWER-B 0.87499
***UPPER-B 1.8899
***VIS-VCMU 8
***LOWER-B 1.2701
***UPPER-B 2.7434
***VIS-VCMU 9
***LOWER-B 1.5842
***UPPER-B 3.4219
***VIS-VCMU 10
***LOWER-B 1.8406
***UPPER-B 3.9758
***PC 10 9 8 7 6 5
***LOWER-B 10 9 8 7 6 5
** 4.3542 6.1693 7.9281 11.246 17.23 25.598
***UPPER-B 10 9 8 7 6 5
** 6.5314 7.823 11.024 16.86 25.134 37.295
***VC 10 9 8 7 6 5
***LOWER-B 10 9 8 7 6 5
** 1.8406 1.5842 1.2701 0.87499 0.5251 0.32894
***UPPER-B 10 9 8 7 6 5
** 2.761 2.3763 1.9052 1.3124 0.78765 0.49341

**=-=-=Saturation Pressure_E
***PRESSAT
***LABEL "
***FEED *MIXED 1.0
***KVALUE *INTERNAL
***LEVEL 1
***OUTPUT 1
***PRES 1390.0

```
***TEMP 71.6
***SATFLAG 2
***EXPERIMENTAL
***PSAT  *DATA  1390.0
***WEIGHT  5.0
**

**=-=-=Constant Composition Expansion_E
***CCE
***LABEL    "
***FEED  *MIXED 1.0
***KVALUE  *INTERNAL
***LEVEL 1
***OUTPUT 1
***PRES 1390.0
***TEMP 71.6
***SATFLAG 2
***NCCE 21
***PRES-CCE
**5013.0  4013.0  3013.0  2513.0  2013.0
**1813.0  1613.0  1390.0  1258.0  1211.0
**1155.0  1113.0  1036.0  967.0  856.0
**802.0  692.0  540.0  412.0  233.0
**141.0
***LIQ_VOL    *PERCENT_CV
***EXPERIMENTAL
***ROV *DATA
**0.989536  0.991969  0.994694  0.996202  0.997797
**0.998481  0.999187  1.0  1.007308  1.010593
**1.015103  1.018984  1.027454  1.036908  1.057255
**1.070291  1.10637  1.192596  1.335762  1.898541
**2.872136
***WEIGHT  1.0
**
***DL *DATA
**60.16  60.01  59.85  59.76  59.66
**59.62  59.58  59.53  -1.0  -1.0
**-1.0  -1.0  -1.0  -1.0  -1.0
**-1.0  -1.0  -1.0  -1.0  -1.0
**-1.0
***WEIGHT  4.0
**

**=-=-=Differential Liberation_E
***DIFLIB
***LABEL    "
```

```
***FEED  *MIXED 1.0
***KVALUE  *INTERNAL
***LEVEL 1
***OUTPUT 1
***PRES 5013.0
***TEMP 71.6
***SATFLAG 2
***STP 14.69595
***STT 60.0008
***CONSISTENCYCHECKS    *YES
***NPSTEPS 14
***PRES-DIFL
**4013.0  3013.0  2513.0  2013.0  1813.0
**1613.0  1390.0  1113.0  913.0  713.0
**513.0  313.0  113.0  13.0
***EXPERIMENTAL
***ROV *DATA
**1.0401  1.0426  1.0455  1.0471  1.0488
**1.0495  1.0502  1.0511  1.0456  1.0394
**1.0331  1.0266  1.0196  1.0122  1.0085
***WEIGHT  0.0
**
***GOR *DATA
**116.26  116.26  116.26  116.26  116.26
**116.26  116.26  116.26  94.71  78.3
**60.49  42.32  26.44  8.95  0.0
***WEIGHT  0.0
**
***DL *DATA
**0.9637  0.9613  0.9587  0.9572  0.9557
**0.955  0.9544  0.9536  0.9572  0.9604
**0.9636  0.9669  0.9706  0.9743  0.9768
***WEIGHT  25.0
**
***ZV *DATA
**-1.0  -1.0  -1.0  -1.0  -1.0
**-1.0  -1.0  -1.0  0.8727  0.8913
**0.9115  0.934  0.9584  0.9845  0.9981
***WEIGHT  0.0
**
***FVF *DATA
**-1.0  -1.0  -1.0  -1.0  -1.0
**-1.0  -1.0  -1.0  0.0117  0.0145
**0.0189  0.0267  0.0442  0.1177  0.5855
***WEIGHT  0.0
**
```

```
***SGV *DATA
**-1.0  -1.0  -1.0  -1.0  -1.0
**-1.0  -1.0  -1.0  0.5899  0.5869
**0.5818  0.5761  0.5705  0.569  0.5779
***WEIGHT  0.0
**
***MUL *DATA
**-1.0  -1.0  -1.0  -1.0  7056.6
**6446.0  5863.0  5260.0  6308.0  7559.0
**8819.0  10230.0  11835.0  14463.0  17753.0
***WEIGHT  10.0
**
***MUV *DATA
**-1.0  -1.0  -1.0  -1.0  -1.0
**-1.0  -1.0  -1.0  0.013  0.01254
**0.01215  0.01184  0.01159  0.01139  0.01128
***WEIGHT  0.0
**
***API  *DATA  12.24
***WEIGHT  0.0
***DR  *DATA  0.9844
***WEIGHT  10.0

**=-=-=Separator_E
***SEPARATOR
***LABEL    "
***FEED  *MIXED 1.0
***KVALUE  *INTERNAL
***LEVEL 1
***OUTPUT 1
***PRES 1390.0
***TEMP 71.6
***SATFLAG 2
***STP 14.69595
***STT 60.0
***NSEP 0
****NC  10  10
****NUMBER_OF_COLUMNS  1
***VAPCOMP
**0.0
**0.0
**0.0
**0.0
**0.0
**0.0
**0.0
```

```
**0.0
**0.0
**0.0
***EXPERIMENTAL
***GOR  *DATA  114.96
***WEIGHT  0.0
***FVF  *DATA  1.06
***WEIGHT  10.0
***API  *DATA  12.36
***WEIGHT  1.0

**=-=-=End Regression_E
**REM     End of Regression Block
***STARTREG

**=-=-=Separator_E
***SEPARATOR
***LABEL    "
***FEED  *MIXED 1.0
***KVALUE  *INTERNAL
***LEVEL 1
***OUTPUT 1
***PRES 1390.0
***TEMP 71.6
***SATFLAG 2
***STP 14.69595
***STT 60.0
***NSEP 0
****NC  10  10
****NUMBER_OF_COLUMNS  1
***VAPCOMP
**0.0
**0.0
**0.0
**0.0
**0.0
**0.0
**0.0
**0.0
**0.0
**0.0
***EXPERIMENTAL
***GOR  *DATA  114.96
***WEIGHT  1.0
***FVF  *DATA  1.0497
***WEIGHT  1.0
```

```
***API *DATA 12.36
***WEIGHT 10.0

**=-=-=Differential Liberation_E
***DIFLIB
***LABEL "
***FEED *MIXED 1.0
***KVALUE *INTERNAL
***LEVEL 1
***OUTPUT 1
***PRES 5013.0
***TEMP 71.6
***SATFLAG 2
***STP 14.69595
***STT 60.0008
***CONSISTENCYCHECKS *YES
***NPSTEPS 14
***PRES-DIFL
**4013.0 3013.0 2513.0 2013.0 1813.0
**1613.0 1390.0 1113.0 913.0 713.0
**513.0 313.0 113.0 13.0
***EXPERIMENTAL
***ROV *DATA
**1.0401 1.0426 1.0455 1.0471 1.0488
**1.0495 1.0502 1.0511 1.0456 1.0394
**1.0331 1.0266 1.0196 1.0122 1.0085
***WEIGHT 0.0
**
***GOR *DATA
**116.26 116.26 116.26 116.26 116.26
**116.26 116.26 116.26 94.71 78.3
**60.49 42.32 26.44 8.95 0.0
***WEIGHT 0.0
**
***DL *DATA
**0.9637 0.9613 0.9587 0.9572 0.9557
**0.955 0.9544 0.9536 0.9572 0.9604
**0.9636 0.9669 0.9706 0.9743 0.9768
***WEIGHT 5.0
**
***ZV *DATA
**-1.0 -1.0 -1.0 -1.0 -1.0
**-1.0 -1.0 -1.0 0.8727 0.8913
**0.9115 0.934 0.9584 0.9845 0.9981
***WEIGHT 0.0
**
```

```
***FVF *DATA
**-1.0  -1.0  -1.0  -1.0  -1.0
**-1.0  -1.0  -1.0  0.0117  0.0145
**0.0189  0.0267  0.0442  0.1177  0.5855
***WEIGHT  0.0
**
***SGV *DATA
**-1.0  -1.0  -1.0  -1.0  -1.0
**-1.0  -1.0  -1.0  0.5899  0.5869
**0.5818  0.5761  0.5705  0.569  0.5779
***WEIGHT  0.0
**
***MUL *DATA
**-1.0  -1.0  -1.0  -1.0  7056.6
**6446.0  5863.0  5260.0  6308.0  7559.0
**8819.0  10230.0  11835.0  14463.0  17753.0
***WEIGHT  0.0
**
***MUV *DATA
**-1.0  -1.0  -1.0  -1.0  -1.0
**-1.0  -1.0  -1.0  0.013  0.01254
**0.01215  0.01184  0.01159  0.01139  0.01128
***WEIGHT  0.0
**
***API  *DATA  12.24
***WEIGHT  10.0
***DR  *DATA  0.9844
***WEIGHT  1.0
**=-=-=Constant Composition Expansion_E
***CCE
***LABEL    "
***FEED  *MIXED 1.0
***KVALUE  *INTERNAL
***LEVEL 1
***OUTPUT 1
***PRES 1390.0
***TEMP 71.6
***SATFLAG 2
***NCCE 21
***PRES-CCE
**5013.0  4013.0  3013.0  2513.0  2013.0
**1813.0  1613.0  1390.0  1258.0  1211.0
**1155.0  1113.0  1036.0  967.0  856.0
**802.0  692.0  540.0  412.0  233.0
**141.0
***LIQ_VOL    *PERCENT_CV
```

```
***EXPERIMENTAL
***ROV *DATA
**0.989536  0.991969  0.994694  0.996202  0.997797
**0.998481  0.999187  1.0  1.007308  1.010593
**1.015103  1.018984  1.027454  1.036908  1.057255
**1.070291  1.10637  1.192596  1.335762  1.898541
**2.872136
***WEIGHT  1.0
**
***DL *DATA
**60.16  60.01  59.85  59.76  59.66
**59.62  59.58  59.53  -1.0  -1.0
**-1.0  -1.0  -1.0  -1.0  -1.0
**-1.0  -1.0  -1.0  -1.0  -1.0
**-1.0
***WEIGHT  4.0
**
**=-=-=Two-phase Envelope_E
***ENVELOPE
***LABEL    'After regression'
***FEED  *MIXED 1.0
***KVALUE  *INTERNAL
***OUTPUT 1
***STABCHECK *YES
***TRACEBOTH *NO
***X-AXIS     *TEMP
***RANGT     -148.0    1292.0
***Y-AXIS     *PRES
***RANGP     0.0    14695.95
***PRES    14.69595
***TEMP    1000.0
***MAXSP   99
***STEPDIR   0.2
***RANGFV    -10.0    10.0
***NTAB   0
***NQUALITY    4
***QUALITY
**0.0   0.1   0.3   0.5

**=-=-=     END
```